AN ABSTRACT OF THE THESIS OF

Brenton S. Ching for the degree of Master of Science in Nuclear Engineering presented on August 9, 2000. Title: Analysis of Iteration Schemes for Deterministic Transport in Binary Markovian Mixtures.

Abstract approved: Redacted for Privacy

Todd S. Palmer

The Adams-Larsen-Pomraning coupled transport model has been used to describe neutral particle transport in binary stochastic mixtures. Here, the mixing statistics are considered to be homogeneous Markovian processes. While the model is robust, the convergence behavior and efficiency of this coupled model have not been addressed.

Countless iterative methods could be employed to solve the coupled model. In this study, three candidate iterative schemes are analyzed with the Fourier analysis technique. The schemes are tested and implemented with a variety of material data to observe the convergence behaviors. While two schemes appear to be stable and convergent, both can converge slowly in the presence of scattering.

We develop a two-grid acceleration scheme to improve the convergence rate of the fully-implicit iteration scheme. A shape function from the high-order coupled transport equations (fine-grid) is used to collapse cross-sections for an effectively-mixed one-material transport approximation (coarse-grid). In turn, diffusion synthetic acceleration is applied to the coarse-grid transport operator in the event that the effective scattering ratio is near unity.

Theoretical and computational results indicate that this two-grid acceleration technique is highly efficient and effective for improving the convergence rate.

Analysis of Iteration Schemes for Deterministic Transport in Binary Markovian Mixtures

by

Brenton S. Ching

A THESIS

submitted to

Oregon State University

in partial fulfillment of
the requirements for the
degree of

Master of Science

Presented August 9, 2000
Commencement June 2001

Master of Science thesis of Brenton S. Ching presented on August 9, 2000.

APPROVED:

Redacted for Privacy

Major Professor, representing Nuclear Engineering

Redacted for Privacy

Chair of Department of Nuclear Engineering

Redacted for Privacy

Dean of Graduate School

I understand that my thesis will become part of the permanent collection of Oregon State University libraries. My signature below authorizes release of my thesis to any reader upon request.

Redacted for Privacy

Brenton S. Ching, Author

ACKNOWLEDGEMENT

After seven incredible, albeit brief, years at Oregon State University, I have crossed paths with many figures that have profoundly influenced my life to date as well as what may lie ahead. The staff and faculty of the Department of Nuclear Engineering provided a unique student-teacher atmosphere and at the same time, stimulated enthusiasm for the nuclear industry. However, were it not for the advice, encouragement, and opportunities extended by Dr. Todd Palmer, I would not be in the position that I am in today. For two years, I have served Dr. Palmer as a graduate research assistant for which I am extremely grateful. During this period, my exploration into the world of transport theory and numerical methods yielded by far the most interesting, yet challenging experiences.

I would also like to thank the remaining members of my graduate committee at Oregon State University: Dr. Andrew Klein (Nuclear Engineering), Dr. Deborah Pence (Mechanical Engineering), and Dr. Charles Brunner (Forest Products).

The role of Lawrence Livermore National Laboratory (LLNL) must also be recognized as my graduate research was funded through a grant from LLNL. This also paved the way for me to spend an invaluable summer at the laboratory where I had the greatest "internship" work experience. Being able to work closely with very talented scientists was reward in its own right. It was also with the assistance of Dr. Michael Zika of LLNL that I completed a first publication, and his expertise in this field proved extremely valuable. Also at LLNL, David Miller and Frank Graziani have made significant contributions in the stochastic transport area.

Several collaborators at other institutions must also be noted. Dr. Marvin Adams (Texas A&M University) is a tremendous asset to the Nuclear Engineering Department, and is a well respected professor and mentor for good reason. However, I have not yet had the opportunity to personally meet other collaborators such as

Dr. Ed Larsen (University of Michigan) for his insight and direction of our research and transport algorithms. Dr. Kelly Thompson, or "KT," (Texas A&M University and Los Alamos National Laboratory) supplied the *SNAC* code for transport on unstructured meshes. It is our hope to obtain two-dimensional stochastic transport benchmark results using this computer code.

Of course, life as a graduate student is unique in itself. Without my peers and fellow graduate students, my stint as a graduate student here at Oregon State would have been drastically different. Once known as "TMT" (Transport Methods Team) which later evolved into "NESCL" (Nuclear Engineering and Scientific Computing Laboratory), the six or seven original members including myself, have endured numerous research hang-ups and countless break-throughs. Three members in particular, Brad Eccleston, John Gulick, and Kang Seog Kim, have been there with me since the beginning. Brad, John, and I were all in the same position and thus the similarity in our schedules. Their friendship and constructive criticism, both in- and out- of class, helped me throughout the past two years.

Most importantly, however, I must acknowledge the love and support from my family: my parents Donald and Mindy Ching, and brother Barry. Their encouragement to seek out all possible opportunities has led me to Oregon State and the nuclear engineering program. I would also like to thank my grandmother, Margaret Ching, for teaching me the value of education in respect to our family heritage.

Finally, I would like to thank Sarah: my source of inspiration. Her continuous love and encouragement throughout my final years as an undergraduate and now as a graduate student have motivated me to keep striving for my goals.

This work was performed in part under the auspices of the United States Department of Energy by Lawrence Livermore National Laboratory contract #B344348.

TABLE OF CONTENTS

TABLE OF CONTENTS (Continued)

LIST OF FIGURES

LIST OF FIGURES (Continued)

LIST OF TABLES

ANALYSIS OF ITERATION SCHEMES FOR DETERMINISTIC TRANSPORT IN BINARY MARKOVIAN MIXTURES

1 INTRODUCTION

Interest in the field of radiation transport in binary stochastic media has been growing. Here, the "stochasticity" of the problem refers to the probability of finding one of the two materials in the randomly-mixed medium at any point in space and time. In other words, only one material can be present at any given position and time since the materials are not allowed to mix at the atomic level. We thus obtain a background consisting of randomly sized "chunks" of the two materials which are in turn randomly distributed throughout the medium.

This is a significant departure from common practice. Currently, if a medium consists of two or more materials, the properties are flux-volume averaged to conserve reaction rates. This then produces a medium of a single "homogenized" material. Realistically, however, materials in nature have heterogeneous and stochastic properties. While the "homogenized" calculations have generally been acceptable, incorporating the statistics of the problem will yield more accurate results.

Research on this subject could prove invaluable for countless applications. In medicine, for one, optical tomography and image reconstruction are vital for diagnoses. Stochastic models have been suggested to provide more detailed descriptions of imaging through biological tissues [Arr 97]. Geologists have also represented groundwater transport with stochastic models. In this case, the statistics are used to generate geometries of various sediments in two- and three- dimensions [Har 84]. Radiation transport through clear and cloudy atmospheres can be described as a binary stochastic process. Here, the transition probabilities within the multicomponent medium are characterized by a number of statistical models [Tit 90], [Mal 93], [Su 94], [Zuev 95]. Any climate changes could then be predicted from the transmitted and reflected

radiation. In reactor physics, fuel elements have randomly distributed burnable poison grains, but current calculations do not accurately account for this heterogeneity. Moreover, two-phase flow can be considered a mixture of two materials: one for each phase. This is especially evident in the liquid water and vapor mixtures of boiling water reactors. Radiation shielding and protection calculations must also precisely depict the shield properties. For example, concrete is not a homogeneous material, rather it consists of randomly distributed materials such as sand and water.

Although the potential of stochastic transport theory was recognized very early, its complexity prompted most research to focus in the non-stochastic area. The objective of stochastic transport calculations is to determine "ensemble-averaged" (mean) values of the particle intensity by averaging over all physical realizations of the background medium. In doing so, the variance, which describes the deviation of the solution from the mean, and other higher statistical moments could also be computed. Assuming the statistics of the medium are known, each realization is generated through either a deterministic or Monte Carlo procedure. The ensuing transport problem is solved, and the process is repeated for all possible statistical realizations. However, the accuracy of the solutions is directly related to the number of realizations: improved accuracy requires more realizations. Likewise, an infinite amount of realizations would yield a zero error but is computationally impossible.

An approximate model of stochastic transport that already contain the ensemble-averaged particle intensity as an unknown provides a suitable alternative. Levermore et al. [Lev 86] and Pomraning [Pom 86], first derived an exact one-dimensional linear transport equation for the ensemble-averaged angular flux. In the case of a purely-absorbing two-fluid statistical mixture, the resulting solution was shown to agree with the expected exponential attenuation result. Pomraning [Pom 89] later proposed a model of two coupled transport equations for neutral particle transport in a binary Markovian mixture. This robust model could be applied to more general transport

problems, including mixtures of more than two materials. Su and Pomraning also investigated mixtures with non-Markovian mixing properties [Su 93].

Adams et al. [MAda 89] derived a similar coupled transport model (the "Adams-Larsen-Pomraning" model) which treats correlation lengths between zero and infinity. This model is obtained by conserving particle balance across an interface then closed with a simple approximation. While the set of coupled transport equations was derived for arbitrary statistics, the considerations were later restricted to mixtures obeying homogeneous Markov statistics. In these cases, the "no-memory" statistics are identical throughout the system and spatially-independent. In the absence of scattering, the Adams-Larsen-Pomraning model is exact.

While there has been extensive research and literature regarding this coupled transport model, including benchmark calculations [MAda 89] and model comparisons [Mal 92], the issue of efficient iteration schemes for the numerical solution of these equations has yet to be addressed. The Adams-Larsen-Pomraning coupled transport model, similar to the general integro-differential Boltzmann transport equation, can be solved using a number of iterative methods. In this paper, we analyze three such candidate iteration schemes that could be applied to this model. Each scheme is tested on a variety of problems, including those of Adams et al. [MAda 89].

Throughout the transport community, it is widely known that for iterative problems involving highly- or purely- scattering materials, the standard Source Iteration process can converge very slowly, if at all. The test cases include these scattering characteristics, thus our algorithms for solving the Adams-Larsen-Pomraning coupled transport model could be adversely affected. A technique to accelerate the convergence rate is therefore necessary in such instances.

This coupled model is analogous to the multigroup S_N transport equations with neutron upscattering. Adams and Morel [BAda 93] developed a highly-efficient two-

grid acceleration scheme for these problems. We propose a two-grid acceleration technique based on the same algorithm to improve the convergence rate of the fully-implicit method. While the two-grid methods are similar in that both collapse the multi-"group" equations to a single low-order equation, the methods differ in the fact that we apply transport equations for both grids. However, our effectively-mixed low-order transport equation must be accelerated as well: effective scattering ratios near unity will cause the low-order Source Iteration to converge slowly. Diffusion synthetic acceleration (DSA) is a proven, unconditionally stable method which converges much more rapidly than Source Iteration alone.

We perform Fourier analyses of the unaccelerated and accelerated systems with analytic-in-space and discretized-in-space calculations. We also verify these results by implementing our iterative methods and observing their convergence behaviors. The theoretical and computational results indicate that this two-grid acceleration scheme, when applied to the fully-implicit method, greatly improves the convergence rate therefore requiring fewer iterations and computational time.

The remainder of this paper is organized as follows. In Section 2, we derive the Adams-Larsen-Pomraning coupled transport model from the standard three-dimensional transport equation following the development in [MAda 89]. We then apply the assumption of homogeneous Markov mixing statistics to the model. Section 3 contains a description of three candidate iterative methods for the coupled model in one-dimensional slab geometry. This section also includes the results of a Fourier analysis of each of these schemes. Our proposed two-grid acceleration scheme is described and analyzed in Section 4. In Section 5, we derive and implement a diffusion synthetic acceleration system for the coarse-grid transport approximation. We finally submit our conclusions and suggestions for future work in Section 6.

2 ANALYTIC COUPLED BINARY MIXTURE TRANSPORT

In this section, we derive a system of two coupled transport equations to describe particle flow in a binary stochastic mixture. It is this system that we refer to as the "Adams-Larsen-Pomraning" coupled transport model. While we formulate the coupled equations for three-dimensional geometry, we assume time-independent, monoenergetic transport with isotropic scattering. The mixing statistics, though arbitrary, are presumed to be known. For this study, we confine our attention to systems with homogeneous Markov statistics.

2.1 Derivation of the Coupled Transport Model

We begin the derivation from the general time-independent, monoenergetic neutron transport equation with isotropic scattering:

$$\mathbf{\Omega} \cdot \mathbf{\nabla} \psi (\mathbf{r}, \mathbf{\Omega}) + \sigma (\mathbf{r}) \psi (\mathbf{r}, \mathbf{\Omega}) = \frac{\sigma_s (\mathbf{r})}{4\pi} \int_{4\pi} \psi (\mathbf{r}, \mathbf{\Omega}') \, d\Omega' + S (\mathbf{r}, \mathbf{\Omega}) \ , \tag{1}$$

where,

$\mathbf{r}$ = spatial vector,

$\mathbf{\Omega}$ = angular vector,

$\psi(\mathbf{r}, \mathbf{\Omega})$ = angular flux,

$\sigma(\mathbf{r})$ = macroscopic total cross-section,

$\sigma_s(\mathbf{r})$ = macroscopic scattering cross-section,

$S(\mathbf{r}, \mathbf{\Omega})$ = external source.

For a particular realization of the statistics, we consider an arbitrary convex volume, V, which is bounded by the surface, B, and is composed of materials 1 and 2. Performing a particle balance in material 1 in V, for example, equates the gain of particles with the loss of particles. Therefore, we multiply the transport equation

of (1), by a characteristic function for material 1

$$\theta_1(\mathbf{r}) = \begin{cases} 1, & \text{if } \mathbf{r} \text{ is in material 1} \\ 0, & \text{otherwise} \end{cases},$$

and then integrate over the volume, V. The resulting equation is

$$\int_B \theta_1(\mathbf{r})\,[\mathbf{n}\cdot\boldsymbol{\Omega}]\,\psi(\mathbf{r},\boldsymbol{\Omega})\,d\mathbf{s} + \int_\Gamma (\mathbf{n}_1\cdot\boldsymbol{\Omega})\,\psi(\mathbf{r},\boldsymbol{\Omega})\,d\mathbf{s} + \int_V \theta_1(\mathbf{r})\,\sigma_1(\mathbf{r})\,\psi(\mathbf{r},\boldsymbol{\Omega})\,d\mathbf{r}$$

$$= \int_V \theta_1(\mathbf{r})\,\frac{\sigma_{s1}(\mathbf{r})}{4\pi}\int_{4\pi}\psi(\mathbf{r},\boldsymbol{\Omega}')\,d\Omega' d\mathbf{r} + \int_V \theta_1(\mathbf{r})\,S_1(\mathbf{r},\boldsymbol{\Omega})\,d\mathbf{r}\,, \tag{2}$$

where we have defined

$$\left[\begin{array}{c}\text{leakage loss across the}\\ \text{bounding surface } B\end{array}\right] \equiv \int_B \theta_1(\mathbf{r})\,[\mathbf{n}\cdot\boldsymbol{\Omega}]\,\psi(\mathbf{r},\boldsymbol{\Omega})\,d\mathbf{s}\,, \tag{3a}$$

$$\left[\begin{array}{c}\text{leakage loss across the}\\ \text{internal surfaces } \Gamma \text{ in 1}\end{array}\right] \equiv \int_\Gamma [\mathbf{n}_1\cdot\boldsymbol{\Omega}]\,\psi(\mathbf{r},\boldsymbol{\Omega})\,d\mathbf{s}\,. \tag{3b}$$

Here, $\mathbf{n}$ is the normal unit vector pointing at a local surface point on B, while $\mathbf{n}_1$ denotes the local normal unit vector in the *outward* direction from material 1.

Thus far, we have not made any approximations, and for a particular realization, (2) is exact. An *ensemble-averaging* over all the realizations produces a useful description. We now define the parameters

$$p_1(\mathbf{r}) = \langle\theta_1(\mathbf{r})\rangle\,, \tag{4a}$$

$$\psi_1(\mathbf{r},\boldsymbol{\Omega}) = \frac{\langle\theta_1(\mathbf{r})\,\psi(\mathbf{r},\boldsymbol{\Omega})\rangle}{\langle\theta_1(\mathbf{r})\rangle}\,, \tag{4b}$$

where the $\langle\cdot\rangle$ represents the ensemble-averaged quantities. Also, p_1 is the probability of finding material 1 at position $\mathbf{r}$, and $\psi_1(\mathbf{r},\boldsymbol{\Omega})$ is the ensemble-averaged angular flux given that $\mathbf{r}$ is in material 1.

Ensemble-averaging (2) over all statistical realizations yields

$$\int_B p_1(\mathbf{r})\,[\mathbf{n}\cdot\boldsymbol{\Omega}]\,\psi_1(\mathbf{r},\boldsymbol{\Omega})\,d\mathbf{s} + \left\langle\int_\Gamma (\mathbf{n}_1\cdot\boldsymbol{\Omega})\,\psi(\mathbf{r},\boldsymbol{\Omega})\,d\mathbf{s}\right\rangle + \int_V p_1(\mathbf{r})\,\sigma_1(\mathbf{r})\,\psi_1(\mathbf{r},\boldsymbol{\Omega})\,d\mathbf{r}$$

$$= \int_V p_1(\mathbf{r})\,\frac{\sigma_{s1}(\mathbf{r})}{4\pi}\int_{4\pi}\psi_1(\mathbf{r},\boldsymbol{\Omega}')\,d\Omega' d\mathbf{r} + \int_V p_1(\mathbf{r})\,S_1(\mathbf{r},\boldsymbol{\Omega})\,d\mathbf{r}\,. \tag{5}$$

Note that the averaging operator could be performed on all terms *except* the leakage term across the internal surface Γ. In other words, the volume V and bounding surface B are common to all realizations, but *not* this surface integral.

Next, the divergence theorem allows us to convert the closed surface integral over B into a volume integral, and as the volume approaches zero, we find

$$\begin{aligned}&\boldsymbol{\Omega}\cdot\boldsymbol{\nabla}p_1(\mathbf{r})\,\psi_1(\mathbf{r},\boldsymbol{\Omega})+\sigma_1(\mathbf{r})\,p_1(\mathbf{r})\,\psi_1(\mathbf{r},\boldsymbol{\Omega})\\&\quad=\frac{\sigma_{s1}(\mathbf{r})}{4\pi}\int_{4\pi}p_1(\mathbf{r})\,\psi_1(\mathbf{r},\boldsymbol{\Omega}')\,d\Omega'+p_1(\mathbf{r})\,S_1(\mathbf{r},\boldsymbol{\Omega})+\chi_1(\mathbf{r},\boldsymbol{\Omega})\;,\end{aligned}\tag{6}$$

where

$$\chi_1(\mathbf{r},\boldsymbol{\Omega})=-\lim_{V\to 0}\left[\frac{1}{V}\left\langle\int_\Gamma(\mathbf{n}_1\cdot\boldsymbol{\Omega})\,\psi(\mathbf{r},\boldsymbol{\Omega})\,d\mathbf{s}\right\rangle\right]\;.\tag{7}$$

To this point, we have yet to make any approximations, and our system of (6) is still formally exact for arbitrary statistics. It is in the probabilities p_1 and the coupling terms of (7) that the statistics of the problem are incorporated.

Particle balance across a material interface suggests that $\chi_1(\mathbf{r},\boldsymbol{\Omega})=-\chi_2(\mathbf{r},\boldsymbol{\Omega})$. In turn, we can rewrite (7) as the sum of two integrals corresponding to each direction: $\mathbf{n}_1\cdot\boldsymbol{\Omega}<0$ and $\mathbf{n}_1\cdot\boldsymbol{\Omega}>0$,

$$\chi_1(\mathbf{r},\boldsymbol{\Omega})=\lim_{V\to 0}\frac{1}{V}\left[\left\langle\int_{\Gamma_2}(\mathbf{n}_2\cdot\boldsymbol{\Omega})\,\psi(\mathbf{r},\boldsymbol{\Omega})\,d\mathbf{s}\right\rangle-\left\langle\int_{\Gamma_1}(\mathbf{n}_1\cdot\boldsymbol{\Omega})\,\psi(\mathbf{r},\boldsymbol{\Omega})\,d\mathbf{s}\right\rangle\right]\;.\tag{8}$$

While the second quantity in (8) is the gain of particles incident on material 1 from material 2, the last term is simply the outgoing transmission of particles from material 1, or,

$$T_1=\lim_{V\to 0}\left[\frac{1}{V}\left\langle\int_{\Gamma_1}(\mathbf{n}_1\cdot\boldsymbol{\Omega})\,\psi(\mathbf{r},\boldsymbol{\Omega})\,d\mathbf{s}\right\rangle\right]\;.\tag{9}$$

Multiplying and dividing (9) by the same quantity,

$$T_1=\lim_{V\to 0}\left[\frac{1}{V}\left\langle\int_{\Gamma_1}(\mathbf{n}_1\cdot\boldsymbol{\Omega})\,\psi(\mathbf{r},\boldsymbol{\Omega})\,d\mathbf{s}\right\rangle\times\frac{\left\langle\int_{\Gamma_1}(\mathbf{n}_1\cdot\boldsymbol{\Omega})\,d\mathbf{s}\right\rangle}{\left\langle\int_{\Gamma_1}(\mathbf{n}_1\cdot\boldsymbol{\Omega})\,d\mathbf{s}\right\rangle}\right]\;.\tag{10}$$

We recognize that

$$\frac{1}{V}\left\langle \int_{\Gamma_1} (\mathbf{n}_1 \cdot \mathbf{\Omega})\, d\mathbf{s} \right\rangle$$

is dependent on the statistics, so we represent this as

$$\frac{p_1(\mathbf{r})}{\overline{\Lambda}_1(\mathbf{r},\mathbf{\Omega})} = \frac{1}{V}\left\langle \int_{\Gamma_1} (\mathbf{n}_1 \cdot \mathbf{\Omega})\, d\mathbf{s} \right\rangle , \tag{11}$$

where $\overline{\Lambda}_1(\mathbf{r},\mathbf{\Omega})$ is also a statistically-dependent geometric quantity. We will discuss this term in greater detail later in Section 2.2. The interface ensemble-averaged angular flux, $\overline{\psi}_1(\mathbf{r},\mathbf{\Omega})$ is defined as,

$$\overline{\psi}_1(\mathbf{r},\mathbf{\Omega}) = \frac{\left\langle \int_{\Gamma_1} (\mathbf{n}_1 \cdot \mathbf{\Omega})\, \psi(\mathbf{r},\mathbf{\Omega})\, d\mathbf{s} \right\rangle}{\left\langle \int_{\Gamma_1} (\mathbf{n}_1 \cdot \mathbf{\Omega})\, d\mathbf{s} \right\rangle} , \tag{12}$$

and (10) subsequently simplifies to

$$T_1 = \frac{p_1(\mathbf{r})}{\overline{\Lambda}_1(\mathbf{r},\mathbf{\Omega})}\overline{\psi}_1(\mathbf{r},\mathbf{\Omega}) . \tag{13}$$

We must relate the interface ensemble-averaged angular flux, $\overline{\psi}_1(\mathbf{r},\mathbf{\Omega})$, to the volumetric ensemble-averaged angular flux, $\psi_1(\mathbf{r},\mathbf{\Omega})$, found in (6). To do so, we make the approximation

$$\psi_1(\mathbf{r},\mathbf{\Omega}) \approx \overline{\psi}_1(\mathbf{r},\mathbf{\Omega}) . \tag{14}$$

Thus, (13) becomes

$$T_1 = \frac{p_1(\mathbf{r})}{\overline{\Lambda}_1(\mathbf{r},\mathbf{\Omega})}\psi_1(\mathbf{r},\mathbf{\Omega}) , \tag{15}$$

and the coupling terms, $\chi_1(\mathbf{r},\mathbf{\Omega})$, in (8) reduce to

$$\chi_1(\mathbf{r},\mathbf{\Omega}) = \frac{p_2(\mathbf{r})}{\overline{\Lambda}_2(\mathbf{r},\mathbf{\Omega})}\psi_1(\mathbf{r},\mathbf{\Omega}) - \frac{p_1(\mathbf{r})}{\overline{\Lambda}_1(\mathbf{r},\mathbf{\Omega})}\psi_1(\mathbf{r},\mathbf{\Omega}) . \tag{16}$$

By substituting (16) into (6), we arrive at the first of two transport equations:

$$\begin{aligned}
&\boldsymbol{\Omega}\cdot\boldsymbol{\nabla}p_1\left(\mathbf{r}\right)\psi_1\left(\mathbf{r},\boldsymbol{\Omega}\right)+\sigma_1\left(\mathbf{r}\right)p_1\left(\mathbf{r}\right)\psi_1\left(\mathbf{r},\boldsymbol{\Omega}\right)\\
&\qquad=\frac{\sigma_{s1}\left(\mathbf{r}\right)}{4\pi}\int_{4\pi}p_1\left(\mathbf{r}\right)\psi_1\left(\mathbf{r},\boldsymbol{\Omega}'\right)d\Omega'+p_1\left(\mathbf{r}\right)S_1\left(\mathbf{r},\boldsymbol{\Omega}\right)\\
&\qquad\qquad+\frac{p_2\left(\mathbf{r}\right)}{\overline{\Lambda}_2\left(\mathbf{r},\boldsymbol{\Omega}\right)}\psi_1\left(\mathbf{r},\boldsymbol{\Omega}\right)-\frac{p_1\left(\mathbf{r}\right)}{\overline{\Lambda}_1\left(\mathbf{r},\boldsymbol{\Omega}\right)}\psi_1\left(\mathbf{r},\boldsymbol{\Omega}\right)\ .
\end{aligned}\tag{17}$$

We likewise infer that, by following the same procedure, we could derive a similar equation governing particle balance in material 2,

$$\begin{aligned}
&\boldsymbol{\Omega}\cdot\boldsymbol{\nabla}p_2\left(\mathbf{r}\right)\psi_2\left(\mathbf{r},\boldsymbol{\Omega}\right)+\sigma_2\left(\mathbf{r}\right)p_2\left(\mathbf{r}\right)\psi_2\left(\mathbf{r},\boldsymbol{\Omega}\right)\\
&\qquad=\frac{\sigma_{s2}\left(\mathbf{r}\right)}{4\pi}\int_{4\pi}p_2\left(\mathbf{r}\right)\psi_2\left(\mathbf{r},\boldsymbol{\Omega}'\right)d\Omega'+p_2\left(\mathbf{r}\right)S_2\left(\mathbf{r},\boldsymbol{\Omega}\right)\\
&\qquad\qquad+\frac{p_1\left(\mathbf{r}\right)}{\overline{\Lambda}_1\left(\mathbf{r},\boldsymbol{\Omega}\right)}\psi_1\left(\mathbf{r},\boldsymbol{\Omega}\right)-\frac{p_2\left(\mathbf{r}\right)}{\overline{\Lambda}_2\left(\mathbf{r},\boldsymbol{\Omega}\right)}\psi_2\left(\mathbf{r},\boldsymbol{\Omega}\right)\ .
\end{aligned}\tag{18}$$

Equations (17) and (18) comprise the Adams-Larsen-Pomraning coupled stochastic transport model. Solving this system of equations allows one to calculate the ensemble-averaged angular flux:

$$\left\langle\psi\left(\mathbf{r},\boldsymbol{\Omega}\right)\right\rangle=p_1\left(\mathbf{r}\right)\psi_1\left(\mathbf{r},\boldsymbol{\Omega}\right)+p_2\left(\mathbf{r}\right)\psi_2\left(\mathbf{r},\boldsymbol{\Omega}\right)\ .\tag{19}$$

It is worthwhile to re-emphasize several aspects of this derivation. First, no approximations were made until (14), so the system given by (6) is exact. Furthermore, the system has been derived for arbitrary statistics and is therefore independent from the type of statistical model chosen.

2.2 Markov Statistics

Now that we have established the coupled set of transport equations, we must address the treatment of the statistics so that we can formally close the system. In

this study, we describe the mixing properties with homogeneous Markov statistics to formulate expressions for the probabilities, p_1 and p_2, and for the statistical quantities, $\overline{\Lambda}_1(\mathbf{r}, \mathbf{\Omega})$ and $\overline{\Lambda}_2(\mathbf{r}, \mathbf{\Omega})$.

Although particle transport in itself is a stochastic process, it is vital that we make a careful clarification. In our use of the term "stochastic process," we refer to the properties of a binary mixture as a function of space. Therefore, while we are not absolutely certain which material is present at a particular location, we do know the probability of a given material being present.

A special class of stochastic processes are predominantly found in physics and chemistry. These processes are known as *Markov*, or "no-memory," processes where the underlying feature is that the conditional probability density could be determined without knowledge and/or dependence of the values at prior or subsequent locations. In other words, finding a particle at a particular location is not dependent on where it was previously, nor does it have an influence on its next location. For the case of Markov statistics, $\overline{\Lambda}_{(1,2)}(\mathbf{r}, \mathbf{\Omega})$ are the Markov transition lengths for materials 1 and 2, respectively.

A sub-class of a Markov process occurs when the statistics are homogeneous, that is, all points on a line have identical statistical properties and are thus independent of position. Without the dependence, we rewrite the probabilities as

$$p_{(1,2)} = p_{(1,2)}\left(\mathbf{r}\right) , \tag{20}$$

and likewise the transition lengths

$$\overline{\Lambda}_{(1,2)} = \overline{\Lambda}_{(1,2)}\left(\mathbf{r}, \mathbf{\Omega}\right) . \tag{21}$$

Mathematically, we can describe a few relevant statistical parameters. First, let $f_{(1,2)}(\tau)$ represent the probability density function for a segment of length τ in material

1 or 2. In turn,

$$\left[\begin{array}{l}\text{Probability of a segment of material 1 or 2}\\ \text{having a length lying between } \tau \text{ and } \tau + d\tau\end{array}\right] \equiv f_{(1,2)}(\tau)\, d\tau\,. \tag{22}$$

The mean chord length, $\Lambda_{(1,2)}$, or average segment size, in material 1 or 2 is then determined by

$$\Lambda_{(1,2)} = \int_0^\infty \tau' f_{(1,2)}(\tau')\, d\tau'\,, \tag{23}$$

and relates the probabilities $p_{(1,2)}$ of finding each material such that

$$p_1 = \frac{\Lambda_1}{\Lambda_1 + \Lambda_2} \quad \text{and} \quad p_2 = \frac{\Lambda_2}{\Lambda_1 + \Lambda_2}\,, \tag{24}$$

where the mean chord lengths are exponentially distributed as

$$f_{(1,2)}(\tau) = \frac{1}{\Lambda_{(1,2)}} e^{-\tau/\Lambda_{(1,2)}}\,. \tag{25}$$

Pomraning [Pom 91] has shown that in the case of homogeneous Markov statistics, the mean chord lengths $\Lambda_{(1,2)}$ are equal to the Markov transition lengths $\overline{\Lambda}_{(1,2)}$. Thus, if $\overline{\Lambda}_1 = \Lambda_1$ and $\overline{\Lambda}_2 = \Lambda_2$, then (24) is equivalently

$$p_1 = \frac{\overline{\Lambda}_1}{\overline{\Lambda}_1 + \overline{\Lambda}_2} \quad \text{and} \quad p_2 = \frac{\overline{\Lambda}_2}{\overline{\Lambda}_1 + \overline{\Lambda}_2}\,. \tag{26}$$

Likewise,

$$f_{(1,2)}(\tau) = \frac{1}{\overline{\Lambda}_{(1,2)}} e^{-\tau/\overline{\Lambda}_{(1,2)}}\,. \tag{27}$$

Using this statistical model, we represent the two transport equations of the Adams-Larsen-Pomraning coupled stochastic system as:

$$\begin{aligned}&\boldsymbol{\Omega}\cdot\boldsymbol{\nabla} p_1\psi_1(\mathbf{r},\boldsymbol{\Omega}) + \sigma_1(\mathbf{r})\, p_1\psi_1(\mathbf{r},\boldsymbol{\Omega})\\ &= \frac{\sigma_{s1}(\mathbf{r})}{4\pi}\int_{4\pi} p_1\psi_1(\mathbf{r},\boldsymbol{\Omega}')\, d\Omega' + p_1 S_1(\mathbf{r},\boldsymbol{\Omega}) + \frac{p_2}{\Lambda_2}\psi_1(\mathbf{r},\boldsymbol{\Omega}) - \frac{p_1}{\Lambda_1}\psi_1(\mathbf{r},\boldsymbol{\Omega})\end{aligned} \tag{28a}$$

$$\mathbf{\Omega} \cdot \boldsymbol{\nabla} p_2 \psi_2 (\mathbf{r}, \mathbf{\Omega}) + \sigma_2 (\mathbf{r}) \, p_2 \psi_2 (\mathbf{r}, \mathbf{\Omega})$$

$$= \frac{\sigma_{s2} (\mathbf{r})}{4\pi} \int_{4\pi} p_2 \psi_2 (\mathbf{r}, \mathbf{\Omega}') \, d\Omega' + p_2 S_2 (\mathbf{r}, \mathbf{\Omega}) + \frac{p_1}{\Lambda_1} \psi_1 (\mathbf{r}, \mathbf{\Omega}) - \frac{p_2}{\Lambda_2} \psi_2 (\mathbf{r}, \mathbf{\Omega}) \ . \quad (28b)$$

We observe several features of these equations. In the limit where the Markov transition lengths (or mean chord lengths) were to increase without bound, the two equations de-couple from one another. On the other hand, if the lengths were to decrease to zero, the influence of the coupling terms would be more pronounced. The effects of these characteristics will be evident in our analyses of Sections 3 and 4.

3 1-D COUPLED STOCHASTIC TRANSPORT

For the remainder of this study, we consider the stochastic transport problem in one-dimensional slab geometry. In this section, we first formulate the appropriate system of equations for the Adams-Larsen-Pomraning coupled transport model. We then discuss three candidate iteration schemes in an attempt to solve the resulting system, and we derive a Fourier analysis for each. The results from the analyses are presented both analytically- and discretized- in space.

3.1 Derivation of the 1-Dimensional Model

We begin by recalling Equations (28a) and (28b) from Section 2.2 which represent the closed system of three-dimensional transport equations:

$$\begin{aligned}
&\boldsymbol{\Omega}\cdot\boldsymbol{\nabla}p_1\psi_1\left(\mathbf{r},\boldsymbol{\Omega}\right)+\sigma_1\left(\mathbf{r}\right)p_1\psi_1\left(\mathbf{r},\boldsymbol{\Omega}\right)\\
&\quad=\frac{\sigma_{s1}\left(\mathbf{r}\right)}{4\pi}\int_{4\pi}p_1\psi_1\left(\mathbf{r},\boldsymbol{\Omega}'\right)d\Omega'+p_1S_1\left(\mathbf{r},\boldsymbol{\Omega}\right)+\frac{p_2}{\Lambda_2}\psi_1\left(\mathbf{r},\boldsymbol{\Omega}\right)-\frac{p_1}{\Lambda_1}\psi_1\left(\mathbf{r},\boldsymbol{\Omega}\right)
\end{aligned}$$

$$\begin{aligned}
&\boldsymbol{\Omega}\cdot\boldsymbol{\nabla}p_2\psi_2\left(\mathbf{r},\boldsymbol{\Omega}\right)+\sigma_2\left(\mathbf{r}\right)p_2\psi_2\left(\mathbf{r},\boldsymbol{\Omega}\right)\\
&\quad=\frac{\sigma_{s2}\left(\mathbf{r}\right)}{4\pi}\int_{4\pi}p_2\psi_2\left(\mathbf{r},\boldsymbol{\Omega}'\right)d\Omega'+p_2S_2\left(\mathbf{r},\boldsymbol{\Omega}\right)+\frac{p_1}{\Lambda_1}\psi_1\left(\mathbf{r},\boldsymbol{\Omega}\right)-\frac{p_2}{\Lambda_2}\psi_2\left(\mathbf{r},\boldsymbol{\Omega}\right).
\end{aligned}$$

In the Cartesian coordinate system, the streaming operator of (28a) and (28b) can be expressed as

$$\boldsymbol{\Omega}\cdot\boldsymbol{\nabla}=\mu\frac{\partial}{\partial x}+\eta\frac{\partial}{\partial y}+\kappa\frac{\partial}{\partial z}, \tag{30}$$

where the direction cosines are defined as dot products of the direction vector for each of the three cases

$$\mu=\boldsymbol{\Omega}\cdot\boldsymbol{e}_x, \qquad \eta=\boldsymbol{\Omega}\cdot\boldsymbol{e}_y, \qquad \kappa=\boldsymbol{\Omega}\cdot\boldsymbol{e}_z.$$

However, in one-dimensional slab geometry, we assume azimuthal symmetry about the x axis. Therefore, the angular flux is independent of variations in the y and z dimensions, and the streaming operator of (30) reduces to a single term

$$\mathbf{\Omega} \cdot \mathbf{\nabla} = \mu \frac{\partial}{\partial x} . \tag{31}$$

From (31), we can rewrite (28a) and (28b) for one-dimensional slab geometry

$$\mu \frac{\partial}{\partial x} p_1 \psi_1 (x, \mu) + \sigma_1 (x) p_1 \psi_1 (x, \mu)$$

$$= \frac{\sigma_{s1} (x)}{2} \int_{-1}^{1} p_1 \psi_1 (x, \mu') \, d\mu' + \frac{|\mu|}{\Lambda_2} p_2 \psi_2 (x, \mu) - \frac{|\mu|}{\Lambda_1} p_1 \psi_1 (x, \mu) , \tag{32a}$$

$$\mu \frac{\partial}{\partial x} p_2 \psi_2 (x, \mu) + \sigma_2 (x) p_2 \psi_2 (x, \mu)$$

$$= \frac{\sigma_{s2} (x)}{2} \int_{-1}^{1} p_2 \psi_2 (x, \mu') \, d\mu' + \frac{|\mu|}{\Lambda_1} p_1 \psi_1 (x, \mu) - \frac{|\mu|}{\Lambda_2} p_2 \psi_2 (x, \mu) . \tag{32b}$$

It is for this system of one-dimensional transport equations that we propose three candidate iteration schemes. However, (32a) and (32b) introduce coupling terms which warrant an explanation. If the average slab thickness of material 1 is Λ_1, then the mean chord length seen by a particle traveling in the direction μ, or $\cos\theta$, within material 1 is $\Lambda_1/|\mu|$. This is illustrated in Figure 1.

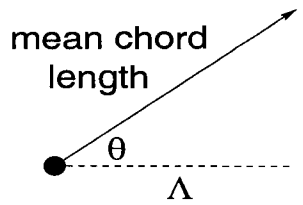

Fig. 1: Particle direction in slab geometry

3.2 Candidate Iterative Schemes

The Adams-Larsen-Pomraning coupled stochastic transport model could be solved through a variety of methods. We present three such iterative procedures here. For

convenience, we use (n) to denote outer iteration levels, and (ℓ) for inner loop iteration levels.

3.2.1 *Fully-Explicit Scheme*

We first consider a fully-explicit iteration scheme by which *both* coupling terms are lagged to the previous iteration level. This scheme incorporates nested iteration loops: an inner loop over the scattering term and an outer loop over the coupling terms. The coupled model is thus represented as:

$$\mu\frac{\partial}{\partial x}p_1\psi_1^{(n+1)}(x,\mu)+\sigma_1(x)\,p_1\psi_1^{(n+1)}(x,\mu)$$

$$=\frac{\sigma_{s1}(x)}{2}\int_{-1}^{1}p_1\psi_1^{(n+1)}(x,\mu')\,d\mu'+\frac{|\mu|}{\Lambda_2}p_2\psi_2^{(n)}(x,\mu)-\frac{|\mu|}{\Lambda_1}p_1\psi_1^{(n)}(x,\mu) \quad (33a)$$

$$\mu\frac{\partial}{\partial x}p_2\psi_2^{(n+1)}(x,\mu)+\sigma_2(x)\,p_2\psi_2^{(n+1)}(x,\mu)$$

$$=\frac{\sigma_{s2}(x)}{2}\int_{-1}^{1}p_2\psi_2^{(n+1)}(x,\mu')\,d\mu'+\frac{|\mu|}{\Lambda_1}p_1\psi_1^{(n)}(x,\mu)-\frac{|\mu|}{\Lambda_2}p_2\psi_2^{(n)}(x,\mu)\,. \quad (33b)$$

It is key to note that we have assumed the scattering term of the inner loop has been converged, and (33) therefore incorporates the latest scalar flux solutions from $(\ell+1)$.

3.2.2 *Partially-Implicit Scheme*

The second iteration scheme involves a partially-implicit treatment of the coupling terms. This scheme is given by:

$$\mu\frac{\partial}{\partial x}p_1\psi_1^{(n+1)}(x,\mu)+\sigma_1(x)\,p_1\psi_1^{(n+1)}(x,\mu)$$

$$=\frac{\sigma_{s1}(x)}{2}\int_{-1}^{1}p_1\psi_1^{(n+1)}(x,\mu')\,d\mu'+\frac{|\mu|}{\Lambda_2}p_2\psi_2^{(n)}(x,\mu)-\frac{|\mu|}{\Lambda_1}p_1\psi_1^{(n+1)}(x,\mu) \quad (34a)$$

$$\mu\frac{\partial}{\partial x}p_2\psi_2^{(n+1)}(x,\mu)+\sigma_2(x)\,p_2\psi_2^{(n+1)}(x,\mu)$$

$$=\frac{\sigma_{s2}(x)}{2}\int_{-1}^{1}p_2\psi_2^{(n+1)}(x,\mu')\,d\mu'+\frac{|\mu|}{\Lambda_1}p_1\psi_1^{(n)}(x,\mu)-\frac{|\mu|}{\Lambda_2}p_2\psi_2^{(n+1)}(x,\mu)\ . \quad (34b)$$

We note that rather than lagging both coupling terms to the previous iteration step, we instead promote only the within-material coupling term. For example, (34a) describes a particle balance in material 1, so its corresponding coupling term is promoted to the $(n+1)$ iteration level. Again, we assume that we have already converged the inner loop over the scattering term within a given tolerance.

3.2.3 Fully-Implicit Scheme

Since the partially-implicit and fully-explicit iteration schemes lag one or both of the coupling terms, we instead introduce a fully-implicit scheme to eliminate the necessity for nested iteration loops. This coupled model can be written as:

$$\mu\frac{\partial}{\partial x}p_1\psi_1^{(\ell+1)}(x,\mu)+\sigma_1(x)\,p_1\psi_1^{(\ell+1)}(x,\mu)$$

$$=\frac{\sigma_{s1}(x)}{2}\int_{-1}^{1}p_1\psi_1^{(\ell)}(x,\mu')\,d\mu'+\frac{|\mu|}{\Lambda_2}p_2\psi_2^{(\ell+1)}(x,\mu)-\frac{|\mu|}{\Lambda_1}p_1\psi_1^{(\ell+1)}(x,\mu) \quad (35a)$$

$$\mu\frac{\partial}{\partial x}p_2\psi_2^{(\ell+1)}(x,\mu)+\sigma_2(x)\,p_2\psi_2^{(\ell+1)}(x,\mu)$$

$$=\frac{\sigma_{s2}(x)}{2}\int_{-1}^{1}p_2\psi_2^{(\ell)}(x,\mu')\,d\mu'+\frac{|\mu|}{\Lambda_1}p_1\psi_1^{(\ell+1)}(x,\mu)-\frac{|\mu|}{\Lambda_2}p_2\psi_2^{(\ell+1)}(x,\mu)\ . \quad (35b)$$

We see that this coupled system can now be solved using the Source Iteration (SI) technique: we first guess the scattering terms at (ℓ) and then iterate until convergence.

3.3 Analysis

The Fourier analysis technique is a very powerful tool for investigating iteration schemes. Its concept is straightforward: we wish to represent a matrix system in

terms of iteration operators and eigenvalues. By computing the eigenvalues, ω, for each Fourier mode, λ, we can predict the convergence behavior and effectiveness of a given iteration scheme. We define the spectral radius ρ as the maximum of the eigenvalues corresponding to the iteration operator:

$$\rho = \sup_{\lambda} |\omega(\lambda)| . \tag{36}$$

The value of the spectral radius indicates the amount by which the error is reduced from iteration to iteration

$$\rho \longrightarrow \begin{cases} \text{converges}, & \text{for } \rho < 1 \\ \text{fails to converge}, & \text{for } \rho = 1 \\ \text{diverges}, & \text{for } \rho > 1 \end{cases} .$$

Therefore, we must develop an iteration scheme where, for convergence, the magnitude of the error decreases between subsequent iterations.

3.3.1 Fully-Explicit Scheme

Subtracting (33) from (32) yields an exact system for the iterate errors:

$$\mu \frac{\partial}{\partial x} p_1 \epsilon_1^{(n+1)}(x,\mu) + \sigma_1(x)\, p_1 \epsilon_1^{(n+1)}(x,\mu)$$

$$= \frac{\sigma_{s1}(x)}{2} \int_{-1}^{1} p_1 \epsilon_1^{(n+1)}(x,\mu')\, d\mu' + \frac{|\mu|}{\Lambda_2} p_2 \epsilon_2^{(n)}(x,\mu) - \frac{|\mu|}{\Lambda_1} p_1 \epsilon_1^{(n)}(x,\mu) \tag{37a}$$

$$\mu \frac{\partial}{\partial x} p_2 \epsilon_2^{(n+1)}(x,\mu) + \sigma_2(x)\, p_2 \epsilon_2^{(n+1)}(x,\mu)$$

$$= \frac{\sigma_{s2}(x)}{2} \int_{-1}^{1} p_2 \epsilon_2^{(n+1)}(x,\mu')\, d\mu' + \frac{|\mu|}{\Lambda_1} p_1 \epsilon_1^{(n)}(x,\mu) - \frac{|\mu|}{\Lambda_2} p_2 \epsilon_2^{(n)}(x,\mu) , \tag{37b}$$

where

$$\epsilon_1^{(n+1)}(x,\mu) = \psi_1(x,\mu) - \psi_1^{(n+1)}(x,\mu) \tag{38a}$$

$$\epsilon_2^{(n+1)}(x,\mu) = \psi_2(x,\mu) - \psi_2^{(n+1)}(x,\mu) . \tag{38b}$$

We assume the solution to the error equation of (37) can be expressed as the Fourier ansatz:

$$p_1\epsilon_1^{(n)}(x,\mu) \cong \omega^{(n)}\xi_1(\mu)\, e^{i\lambda x} \tag{39a}$$

$$p_2\epsilon_2^{(n)}(x,\mu) \cong \omega^{(n)}\xi_2(\mu)\, e^{i\lambda x}\,. \tag{39b}$$

Here we have defined ω as the iteration eigenvalue, $\xi(\mu)$ as its eigenvector, λ as the Fourier mode, and i as the imaginary number $\sqrt{-1}$. Substituting this relationship into (37) yields the eigensystem:

$$\omega\left[\left(i\mu\lambda+\sigma_1(x)\right)\xi_1(\mu)-\frac{\sigma_{s1}(x)}{2}\int_{-1}^{1}\xi_1(\mu')\,d\mu'\right]=\frac{|\mu|}{\Lambda_2}\xi_2(\mu)-\frac{|\mu|}{\Lambda_1}\xi_1(\mu) \tag{40a}$$

$$\omega\left[\left(i\mu\lambda+\sigma_2(x)\right)\xi_2(\mu)-\frac{\sigma_{s2}(x)}{2}\int_{-1}^{1}\xi_2(\mu')\,d\mu'\right]=\frac{|\mu|}{\Lambda_1}\xi_1(\mu)-\frac{|\mu|}{\Lambda_2}\xi_2(\mu)\,. \tag{40b}$$

3.3.2 Partially-Implicit Scheme

Subtracting (34) from (32) results in another exact system for the iterate errors:

$$\begin{aligned}&\mu\frac{\partial}{\partial x}p_1\epsilon_1^{(n+1)}(x,\mu)+\sigma_1(x)\,p_1\epsilon_1^{(n+1)}(x,\mu)\\&=\frac{\sigma_{s1}(x)}{2}\int_{-1}^{1}p_1\epsilon_1^{(n+1)}(x,\mu')\,d\mu'+\frac{|\mu|}{\Lambda_2}p_2\epsilon_2^{(n)}(x,\mu)-\frac{|\mu|}{\Lambda_1}p_1\epsilon_1^{(n+1)}(x,\mu)\end{aligned} \tag{41a}$$

$$\begin{aligned}&\mu\frac{\partial}{\partial x}p_2\epsilon_2^{(n+1)}(x,\mu)+\sigma_2(x)\,p_2\epsilon_2^{(n+1)}(x,\mu)\\&=\frac{\sigma_{s2}(x)}{2}\int_{-1}^{1}p_2\epsilon_2^{(n+1)}(x,\mu')\,d\mu'+\frac{|\mu|}{\Lambda_1}p_1\epsilon_1^{(n)}(x,\mu)-\frac{|\mu|}{\Lambda_2}p_2\epsilon_2^{(n+1)}(x,\mu)\,.\end{aligned} \tag{41b}$$

Assuming the errors can again be represented with the Fourier ansatz of (39), the eigenvalue problem becomes:

$$\omega\left[\left(i\mu\lambda+\sigma_1(x)+\frac{|\mu|}{\Lambda_1}\right)\xi_1(\mu)-\frac{\sigma_{s1}(x)}{2}\int_{-1}^{1}\xi_1(\mu')\,d\mu'\right]=\frac{|\mu|}{\Lambda_2}\xi_2(\mu) \tag{42a}$$

$$\omega\left[\left(i\mu\lambda+\sigma_2(x)+\frac{|\mu|}{\Lambda_2}\right)\xi_2(\mu)-\frac{\sigma_{s2}(x)}{2}\int_{-1}^{1}\xi_2(\mu')\,d\mu'\right]=\frac{|\mu|}{\Lambda_1}\xi_1(\mu)\ . \tag{42b}$$

3.3.3 *Fully-Implicit Scheme*

Subtracting (35) from (32) gives an exact equation for the iterate errors:

$$\mu\frac{\partial}{\partial x}p_1\epsilon_1^{(\ell+1)}(x,\mu)+\sigma_1(x)\,p_1\epsilon_1^{(\ell+1)}(x,\mu)$$

$$=\frac{\sigma_{s1}(x)}{2}\int_{-1}^{1}p_1\epsilon_1^{(\ell)}(x,\mu')\,d\mu'+\frac{|\mu|}{\Lambda_2}p_2\epsilon_2^{(\ell+1)}(x,\mu)-\frac{|\mu|}{\Lambda_1}p_1\epsilon_1^{(\ell+1)}(x,\mu) \tag{43a}$$

$$\mu\frac{\partial}{\partial x}p_2\epsilon_2^{(\ell+1)}(x,\mu)+\sigma_2(x)\,p_2\epsilon_2^{(\ell+1)}(x,\mu)$$

$$=\frac{\sigma_{s2}(x)}{2}\int_{-1}^{1}p_2\epsilon_2^{(\ell)}(x,\mu')\,d\mu'+\frac{|\mu|}{\Lambda_1}p_1\epsilon_1^{(\ell+1)}(x,\mu)-\frac{|\mu|}{\Lambda_2}p_2\epsilon_2^{(\ell+1)}(x,\mu)\ , \tag{43b}$$

where

$$\epsilon_1^{(\ell+1)}(x,\mu)=\psi_1(x,\mu)-\psi_1^{(\ell+1)}(x,\mu) \tag{44a}$$

$$\epsilon_2^{(\ell+1)}(x,\mu)=\psi_2(x,\mu)-\psi_2^{(\ell+1)}(x,\mu)\ . \tag{44b}$$

We substitute similar Fourier ansatz of (39) into (43) to arrive at the eigenvalue system:

$$\omega\left[\xi_1(\mu)\left(i\mu\lambda+\sigma_1(x)+\frac{|\mu|}{\Lambda_1}\right)-\frac{|\mu|}{\Lambda_2}\xi_2(\mu)\right]=\frac{\sigma_{s1}(x)}{2}\int_{-1}^{1}\xi_1(\mu')\,d\mu' \tag{45a}$$

$$\omega\left[\xi_2(\mu)\left(i\mu\lambda+\sigma_2(x)+\frac{|\mu|}{\Lambda_2}\right)-\frac{|\mu|}{\Lambda_1}\xi_1(\mu)\right]=\frac{\sigma_{s2}(x)}{2}\int_{-1}^{1}\xi_2(\mu')\,d\mu'\,. \tag{45b}$$

This system is similar to Source Iteration when applied to a two spatial unknown per zone slab geometry transport discretization such as the linear discontinuous (LD) method.

3.4 Results

We now compare our Fourier analyses of these candidate iteration schemes. The material data for σ, σ_s, and Λ were taken from the benchmark cases of Adams et al. [MAda 89] such that the ensemble-averaged total cross-section, $\langle\sigma\rangle$, is equal to unity. Table 1 lists the σ, σ_s, Λ, and scattering ratio, c, data. For each material, the cross-sections $\sigma(x)$ and $\sigma_s(x)$ were assumed to be spatially homogeneous, or in other words,

$$\sigma_{(1,2)}(x) = \sigma_{(1,2)} \quad \text{and} \quad \sigma_{s(1,2)}(x) = \sigma_{s(1,2)} .$$

Furthermore, with Discrete Ordinates we approximate the integral over all angles to calculate the scalar terms. For example, the scalar fluxes are:

$$\begin{aligned} \phi(x) &= \int_{-1}^{1} \psi(x,\mu')\, d\mu' \\ &\cong \sum_{m=1}^{N} \mathrm{w}_m \psi(x,\mu_m) , \end{aligned} \tag{46}$$

where N is the order of the quadrature set, and we have normalized the weights, w, to satisfy

$$\sum_{n=1}^{N} \mathrm{w}_n = 2 . \tag{47}$$

The unaccelerated calculations correspond to the problem:

1. one-dimensional slab geometry
2. S_4 Gauss-Legendre quadrature set
3. steady-state

Table 1: Material data

case #:	σ_1:	c_1:	Λ_1:	σ_2:	c_2:	Λ_2:
1	10/99	0.0	99/100	100/11	1.0	11/100
2	10/99	1.0	99/100	100/11	0.0	11/100
3	10/99	0.9	99/100	100/11	0.9	11/100
4	10/99	0.0	99/10	100/11	1.0	11/10
5	10/99	1.0	99/10	100/11	0.0	11/10
6	10/99	0.9	99/10	100/11	0.9	11/10
7	2/101	0.0	101/20	200/101	1.0	101/20
8	2/101	1.0	101/20	200/101	0.0	101/20
9	2/101	0.9	101/20	200/101	0.9	101/20

3.4.1 Analytic Results

The analytic-in-space analyses were performed using the MAPLE-V mathematics package on a Hewlett Packard B-class workstation at Oregon State University. It is important to note that while the spatial variable has been treated analytically, we opt to approximate the integral in the scattering term with the Discrete Ordinates method. For the remainder of this study, we use the S_4 Gauss-Legendre quadrature set. The analytic analyses also assume an infinite medium.

After extensive numerical analysis, the fully-explicit scheme represented by (33) appears to be unstable, that is, the spectral radii were in excess of 1.0. In other words, the errors from subsequent iterations on the coupling terms were not converging but were rather increasing in magnitude. This behavior was demonstrated on numerous test cases, including the nine benchmark cases, and the fully-explicit scheme was therefore abandoned.

On the other hand, we have analyzed the partially- and fully- implicit methods of (34) and (35) for a large number of problems with a variety of physical data, and we have concluded that both methods were stable in all cases. While this is not a proof of stability, it strongly suggests that these methods are stable. Figures 2

through 10 show the behavior of both implicit schemes. In some cases, it may appear that the partially-implicit method has a smaller spectral radius than the fully-implicit method. However, we must remark that the partially-implicit spectral radii of our analyses actually measure the behavior of the outer iteration loop over the coupling terms alone; it does not account for the convergence of the scattering term in the inner iteration loop. Conversely, the analysis of the fully-implicit scheme effectively observes the behavior of the *entire* scheme since nested iteration loops were no longer required.

We can see that the spectral radius for each case occurs when $\lambda = 0$, otherwise known as the "flat mode." Therefore, while stable and convergent, this method can converge slowly in some cases. We conclude that the fully-implicit iteration scheme is the superior option, and we direct our focus on this method for the remainder of this study.

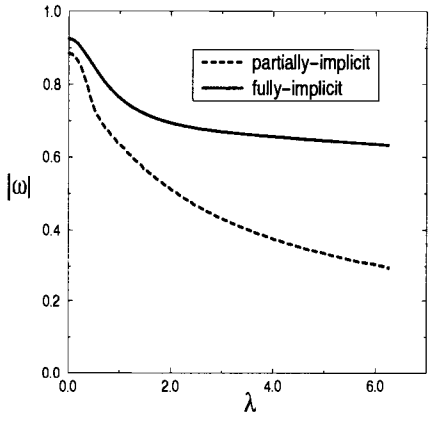

Fig. 2: Eigenvalues of the two stable methods (case 1)

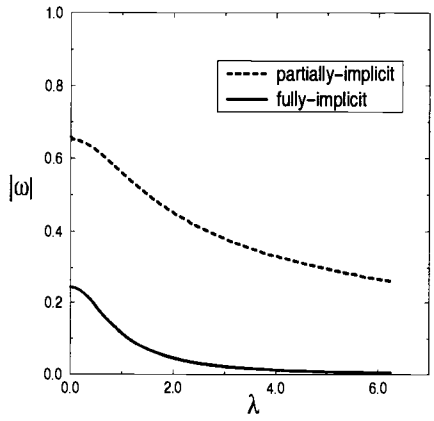

Fig. 3: Eigenvalues of the two stable methods (case 2)

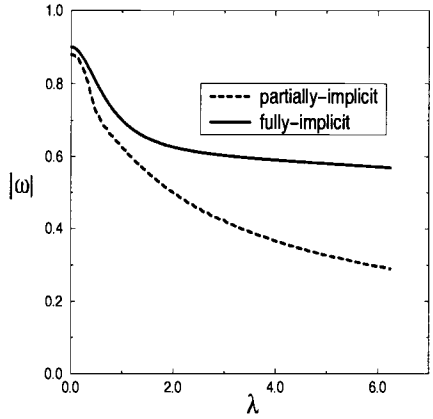

Fig. 4: Eigenvalues of the two stable methods (case 3)

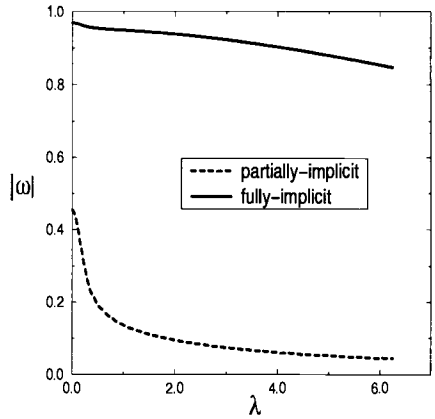

Fig. 5: Eigenvalues of the two stable methods (case 4)

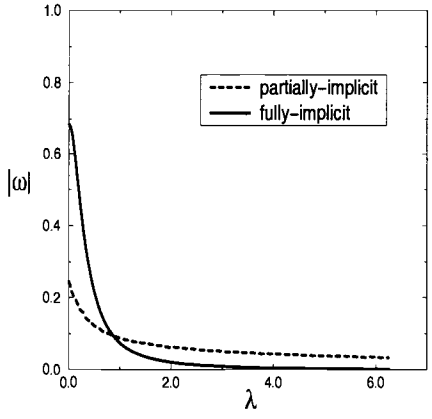

Fig. 6: Eigenvalues of the two stable methods (case 5)

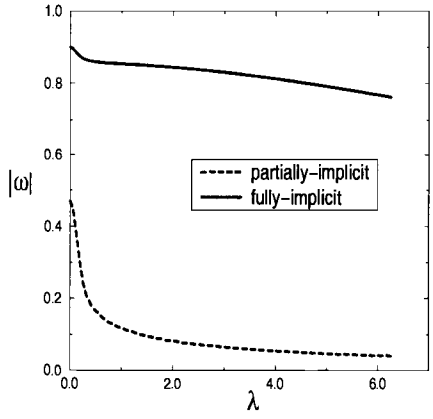

Fig. 7: Eigenvalues of the two stable methods (case 6)

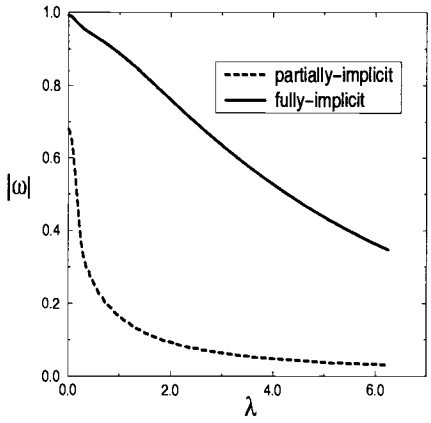

Fig. 8: Eigenvalues of the two stable methods (case 7)

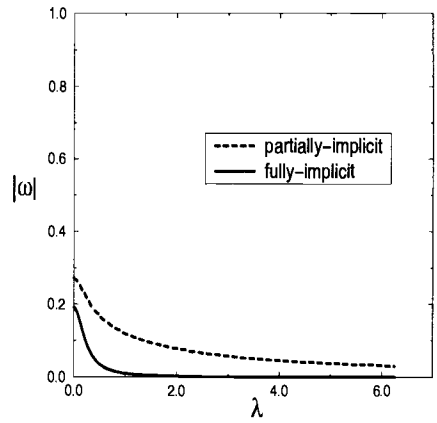

Fig. 9: Eigenvalues of the two stable methods (case 8)

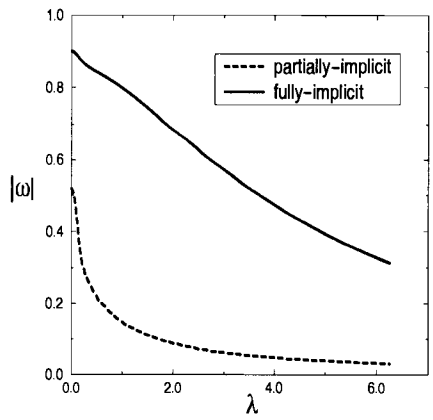

Fig. 10: Eigenvalues of the two stable methods (case 9)

3.4.2 Discretized Results

We now verify the fully-implicit analytic results using a FORTRAN-90 discretized-in-space code which was run on Compaq AlphaServer 4100 Model 5/533 systems at Lawrence Livermore National Laboratory. However, aside from the treatment of the spatial variable, the discretized analysis also assumes that a slab thickness of 5000 cm is sufficient to approximate an infinite medium.

We have chosen to handle the spatial variable with the diamond-difference (DD) discretization technique. Its stencil is shown in Figure 11. The DD discretization relates the cell-edge fluxes to the cell-averaged fluxes by

$$\psi_{k,m} = \frac{1}{2}\left[\psi_{k+1/2,m} + \psi_{k-1/2,m}\right] \tag{48a}$$

$$\phi_k = \frac{1}{2}\left[\phi_{k+1/2} + \phi_{k-1/2}\right] , \tag{48b}$$

where for convenience, we have used subscripts to denote zone midpoints (k), zone edges ($k \pm 1/2$), and ordinates (m). In accordance with Adams et al. [MAda 89], we imposed a restriction on the maximum zone size such that:

$$\Delta x \leq \frac{1}{5\sigma_1}\,|\mu_m|_{min} \quad \text{or} \quad \Delta x \leq \frac{1}{5\sigma_2}\,|\mu_m|_{min} , \tag{49}$$

whichever is the most limiting case.

To obtain the coupled set of DD transport equations, we first integrate the system

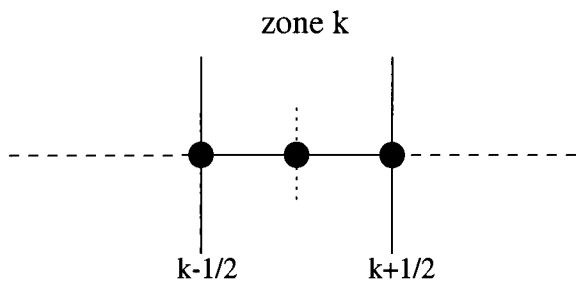

Fig. 11: Diamond-difference discretization stencil

of (35) between zone edges $x_{k-1/2}$ and $x_{k+1/2}$:

$$\mu_m \left[p_1\psi^{(\ell+1)}_{1,k+1/2,m} - p_1\psi^{(\ell+1)}_{1,k-1/2,m}\right] + \left[\sigma_1 + \frac{|\mu_m|}{\Lambda_1}\right]\Delta x p_1\psi^{(\ell+1)}_{1,k,m}$$

$$-\frac{|\mu_m|}{\Lambda_2}\Delta x p_2\psi^{(\ell+1)}_{2,k,m} = \frac{1}{2}\sigma_{s1}\Delta x \sum_{m=1}^{N} \mathrm{w}_m p_1\psi^{(\ell)}_{1,k,m} \tag{50a}$$

$$\mu_m \left[p_2\psi^{(\ell+1)}_{2,k+1/2,m} - p_2\psi^{(\ell+1)}_{2,k-1/2,m}\right] + \left[\sigma_2 + \frac{|\mu_m|}{\Lambda_2}\right]\Delta x p_2\psi^{(\ell+1)}_{2,k,m}$$

$$-\frac{|\mu_m|}{\Lambda_1}\Delta x p_1\psi^{(\ell+1)}_{1,k,m} = \frac{1}{2}\sigma_{s2}\Delta x \sum_{m=1}^{N} \mathrm{w}_m p_2\psi^{(\ell)}_{2,k,m}\,. \tag{50b}$$

Substituting (48) into (50) yields

$$\mu_m \left[p_1\psi^{(\ell+1)}_{1,k+1/2,m} - p_1\psi^{(\ell+1)}_{1,k-1/2,m}\right] + \frac{1}{2}\Delta x \left[\sigma_1 + \frac{|\mu_m|}{\Lambda_1}\right]\left[p_1\psi^{(\ell+1)}_{1,k+1/2,m} + p_1\psi^{(\ell+1)}_{1,k-1/2,m}\right]$$

$$-\frac{1}{2}\Delta x\frac{|\mu_m|}{\Lambda_2}\left[p_2\psi^{(\ell+1)}_{2,k+1/2,m} + p_2\psi^{(\ell+1)}_{2,k-1/2,m}\right] = \frac{1}{2}\sigma_{s1}\Delta x \sum_{m=1}^{N} \mathrm{w}_m p_1\psi^{(\ell)}_{1,k,m} \tag{51a}$$

$$\mu_m \left[p_2\psi^{(\ell+1)}_{2,k+1/2,m} - p_2\psi^{(\ell+1)}_{2,k-1/2,m}\right] + \frac{1}{2}\Delta x \left[\sigma_2 + \frac{|\mu_m|}{\Lambda_2}\right]\left[p_2\psi^{(\ell+1)}_{2,k+1/2,m} + p_2\psi^{(\ell+1)}_{2,k-1/2,m}\right]$$

$$-\frac{1}{2}\Delta x\frac{|\mu_m|}{\Lambda_1}\left[p_1\psi^{(\ell+1)}_{1,k+1/2,m} + p_1\psi^{(\ell+1)}_{1,k-1/2,m}\right] = \frac{1}{2}\sigma_{s2}\Delta x \sum_{m=1}^{N} \mathrm{w}_m p_2\psi^{(\ell)}_{2,k,m}\,. \tag{51b}$$

We complete this system of equations through the use of upstream closures such that the exiting edge fluxes from zone k are the incoming edge fluxes for its neighboring zone ($k-1$ or $k+1$, depending on the value of μ_m).

$$\psi_{exit,k\pm1/2,m} = \begin{cases} \psi_{k+1/2,m}, & \mu_m > 0 \\ \psi_{k-1/2,m}, & \mu_m < 0 \end{cases}\,. \tag{52}$$

This allows us to formulate explicit equations for the two unknown exiting edge fluxes during each transport sweep. In other words, while sweeping in a particular direction,

we must solve two equations in each zone:

$$p_1\psi^{(\ell+1)}_{1,k+1/2,m} =$$

$$\left\{\left[\mu_m\Delta x\frac{|\mu_m|}{\Lambda_2}\right]p_2\psi^{(\ell+1)}_{2,k-1/2,m} + \left[\mu_m + \frac{\Delta x}{2}\hat{\sigma}_{2,m}\right]\Delta x p_1 Q^{(\ell)}_{1,k} + \frac{\Delta x^2}{2}\frac{|\mu_m|}{\Lambda_2}p_2 Q^{(\ell)}_{2,k}\right.$$

$$\left. - \left(\left[\mu_m + \frac{\Delta x}{2}\hat{\sigma}_{2,m}\right]\left[-\mu_m + \frac{\Delta x}{2}\hat{\sigma}_{1,m}\right] - \left(\frac{\Delta x}{2}\right)^2\frac{\mu_m^2}{\Lambda_1\Lambda_2}\right)p_1\psi^{(\ell+1)}_{1,k-1/2,m}\right\}$$

$$\Big/\left\{\left[\mu_m + \frac{\Delta x}{2}\hat{\sigma}_{2,m}\right]\left[\mu_m + \frac{\Delta x}{2}\hat{\sigma}_{1,m}\right] - \left(\frac{\Delta x}{2}\right)^2\frac{\mu_m^2}{\Lambda_1\Lambda_2}\right\}, \quad \mu_m > 0 \qquad (53a)$$

$$p_2\psi^{(\ell+1)}_{2,k+1/2,m} =$$

$$\left\{\left[\mu_m\Delta x\frac{|\mu_m|}{\Lambda_1}\right]p_1\psi^{(\ell+1)}_{1,k-1/2,m} + \left[\mu_m + \frac{\Delta x}{2}\hat{\sigma}_{1,m}\right]\Delta x p_2 Q^{(\ell)}_{2,k} + \frac{\Delta x^2}{2}\frac{|\mu_m|}{\Lambda_1}p_1 Q^{(\ell)}_{1,k}\right.$$

$$\left. - \left(\left[\mu_m + \frac{\Delta x}{2}\hat{\sigma}_{1,m}\right]\left[-\mu_m + \frac{\Delta x}{2}\hat{\sigma}_{2,m}\right] - \left(\frac{\Delta x}{2}\right)^2\frac{\mu_m^2}{\Lambda_1\Lambda_2}\right)p_2\psi^{(\ell+1)}_{2,k-1/2,m}\right\}$$

$$\Big/\left\{\left[\mu_m + \frac{\Delta x}{2}\hat{\sigma}_{2,m}\right]\left[\mu_m + \frac{\Delta x}{2}\hat{\sigma}_{1,m}\right] - \left(\frac{\Delta x}{2}\right)^2\frac{\mu_m^2}{\Lambda_1\Lambda_2}\right\}, \quad \mu_m > 0 \qquad (53b)$$

where

$$Q^{(\ell)}_{(1,2),k} = \frac{1}{2}\sigma_{s(1,2)}\phi^{(\ell)}_{(1,2),k}$$

$$\hat{\sigma}_{(1,2),k,m} = \sigma_{(1,2)} + \frac{|\mu_m|}{\Lambda_{(1,2)}}.$$

After a complete sweep ($\mu > 0$ and $\mu < 0$), we calculate the cell-averaged scalar fluxes from (48) and (46), and then the resulting ensemble-averaged scalar fluxes for that iteration according to (19)

$$\langle\phi^{(\ell+1)}_k\rangle = p_1\phi^{(\ell+1)}_{1,k} + p_2\phi^{(\ell+1)}_{2,k}. \qquad (54)$$

In the absence of *all* sources, we expect scalar flux solutions of zero in each material. By using random initial guesses for the scalar fluxes we excite all the possible error

modes, and we then measure the spectral radius, ρ, as we iterate towards the known solution. The spectral radius was calculated using L_2-norms of the ensemble-averaged scalar flux solutions from subsequent iterations:

$$\rho_k^{(\ell+1)} = \left[\frac{\sum \Delta x \langle \phi_k^{(\ell+1)} \rangle^2}{\sum \Delta x \langle \phi_k^{(\ell)} \rangle^2} \right]^{1/2} . \tag{55}$$

Table 2 compares the results of the discretized analyses with the analytic predictions. We observe that the discretized, computational calculations are generally less than the corresponding analytic, theoretical results. This is due primarily to the truncation of the infinite slab where particles could be "lost" through leakage out of the slab. For an infinite slab, no particles are lost. In case 6, the computational $|\rho|$ is greater than the theoretical $|\rho|$ which may be a result of machine precision and/or round-off error.

Table 2: Performance of the unaccelerated, fully-implicit iteration scheme

case #:	theoretical $\|\rho\|$:	computational $\|\rho\|$:	relative error [%]:
1	0.924619	0.92461	-0.00097
2	0.246187	0.24616	-0.01097
3	0.900000	0.89998	-0.00222
4	0.968480	0.96847	-0.00103
5	0.684799	0.68470	-0.01446
6	0.900000	0.90012	+0.01333
7	0.991910	0.99190	-0.00101
8	0.191045	0.19095	-0.04973
9	0.900000	0.89997	-0.00333

4 A TWO-GRID ACCELERATION SCHEME

The results of our previous Fourier analysis show that the convergence of the fully-implicit method can be slow for cases where the optically-thick material is purely-scattering. Therefore, a scheme to accelerate the convergence rate is necessary for the efficient solution of these problems.

The Adams-Larsen-Pomraning coupled system is analogous to a two-group neutron transport problem with upscattering. For such cases, an iterative scheme would also encounter slow convergence in the presence of purely- or highly- scattering materials. Adams and Morel [BAda 93] developed a two-grid acceleration scheme for the multigroup S_N neutron transport equations with upscattering. This method first approximates the multigroup transport equations with diffusion equations, and then applies a spectral shape function from this multigroup diffusion system ("fine-grid") to calculate group-weighted cross-sections for a one-group diffusion equation ("coarse-grid"). An estimate of the error in the S_N solution iterate is determined from this one-group diffusion equation, and is used to correct and update each scalar flux solution.

Adams and Morel found that the two-grid acceleration scheme was successful in improving the convergence rate at a reasonable and economical computational cost per iteration. Along with a detailed analysis and derivation, Adams and Morel provide theoretical and computational results that demonstrate the efficiency of this scheme.

In this section, we first derive a similar two-grid acceleration system as applied to the Adams-Larsen-Pomraning coupled model, and we also describe the acceleration process. We again compare analytical results to discretized results from the Fourier analyses of our acceleration scheme.

4.1 Two-Grid Derivation

We now proceed to derive the two-grid acceleration method for our set of coupled stochastic transport equations. The fine-grid operator is represented by the coupled transport system of (43) which denotes an exact transport system in terms of iterate errors:

$$\mu\frac{\partial}{\partial x}p_1\epsilon_1^{(\ell+1/2)}(x,\mu)+\sigma_1 p_1\epsilon_1^{(\ell+1/2)}(x,\mu)$$

$$=\frac{\sigma_{s1}}{2}\int_{-1}^{1}p_1\epsilon_1^{(\ell)}(x,\mu')\,d\mu'+\frac{|\mu|}{\Lambda_2}p_2\epsilon_2^{(\ell+1/2)}(x,\mu)-\frac{|\mu|}{\Lambda_2}p_1\epsilon_1^{(\ell+1/2)}(x,\mu) \quad (56a)$$

$$\mu\frac{\partial}{\partial x}p_2\epsilon_2^{(\ell+1/2)}(x,\mu)+\sigma_2 p_2\epsilon_2^{(\ell+1/2)}(x,\mu)$$

$$=\frac{\sigma_{s2}}{2}\int_{-1}^{1}p_2\epsilon_2^{(\ell)}(x,\mu')\,d\mu'+\frac{|\mu|}{\Lambda_1}p_1\epsilon_1^{(\ell+1/2)}(x,\mu)-\frac{|\mu|}{\Lambda_2}p_2\epsilon_2^{(\ell+1/2)}(x,\mu)\,. \quad (56b)$$

From its Fourier system represented by (45), we next obtain the spectral shape function in the form of the eigenvector, $\xi_{(1,2)}(\mu)$ or $\boldsymbol{\xi}$, corresponding to the maximum eigenvalue.

For the derivation of the coarse-grid operator, we begin by adding (56a) and (56b):

$$\mu\frac{\partial}{\partial x}\left[p_1\epsilon_1^{(\ell+1/2)}(x,\mu)+p_2\epsilon_2^{(\ell+1/2)}(x,\mu)\right]+\sigma_1 p_1\epsilon_1^{(\ell+1/2)}(x,\mu)+\sigma_2 p_2\epsilon_2^{(\ell+1/2)}(x,\mu)$$

$$=\frac{\sigma_{s1}}{2}\int_{-1}^{1}p_1\epsilon_1^{(\ell)}(x,\mu')\,d\mu'+\frac{\sigma_{s2}}{2}\int_{-1}^{1}p_2\epsilon_2^{(\ell)}(x,\mu')\,d\mu'\,. \quad (57)$$

We apply the assumption that the error solutions can be represented as the products of a modulation function, $\Upsilon_{eff}(x)$, and the spectral shape function such that:

$$p_{(1,2)}\,\epsilon_{(1,2)}^{(\ell+1/2)}(x,\mu)=\Upsilon_{eff}^{(\ell+1/2)}(x,\mu)\;\xi_{(1,2)}(\mu)\,, \quad (58)$$

where we normalize this spectral shape function

$$\sum_{g=1}^{2}\xi_g(\mu)=1\,. \quad (59)$$

This allows us to rewrite (57):

$$\mu\frac{\partial}{\partial x}\Upsilon_{eff}^{(\ell+1/2)}(x,\mu)+\left[\sigma_1\xi_1(\mu)+\sigma_2\xi_2(\mu)\right]\Upsilon_{eff}^{(\ell+1/2)}(x,\mu)$$

$$=\frac{\sigma_{s1}}{2}\int_{-1}^{1}p_1\epsilon_1^{(\ell)}(x,\mu')\,d\mu'+\frac{\sigma_{s2}}{2}\int_{-1}^{1}p_2\epsilon_2^{(\ell)}(x,\mu')\,d\mu'. \quad (60)$$

From a similar definition of errors as (38),

$$\epsilon_{(1,2)}^{(\ell)}(x,\mu)=\psi_{(1,2)}(x,\mu)-\psi_{(1,2)}^{(\ell)}(x,\mu)\ , \quad (61)$$

we expand (60) for residual terms to ultimately obtain the coarse-grid equation:

$$\mu\frac{\partial}{\partial x}\Upsilon_{eff}^{(\ell+1/2)}(x,\mu)+\sigma_{eff}(\mu)\Upsilon_{eff}^{(\ell+1/2)}(x,\mu)$$

$$=\frac{1}{2}\int_{-1}^{1}\sigma_{s,eff}(\mu')\Upsilon_{eff}^{(\ell)}(x,\mu')d\mu'+\frac{R_1^{(\ell+1/2)}(x)}{2}+\frac{R_2^{(\ell+1/2)}(x)}{2}, \quad (62)$$

where we have defined the residual terms

$$R_{(1,2)}^{(\ell+1/2)}(x)=\sigma_{s(1,2)}p_{(1,2)}\left[\phi_{(1,2)}^{(\ell+1/2)}-\phi_{(1,2)}^{(\ell)}\right]\ , \quad (63)$$

as well as angularly-dependent "effective" cross-sections

$$\sigma_{eff}(\mu) = \sigma_1\xi_1(\mu)+\sigma_2\xi_2(\mu) \quad (64a)$$

$$\sigma_{s,eff}(\mu) = \sigma_{s1}\xi_1(\mu)+\sigma_{s2}\xi_2(\mu)\,. \quad (64b)$$

It is important to note that while we have derived a two-grid acceleration scheme based on the Adams and Morel [BAda 93] two-grid method, the fine- and coarse-grids here involve *transport* equations. As previously mentioned, Adams and Morel approximated the low-order transport equation with a *diffusion* equation.

4.2 Two-Grid Procedure

The acceleration scheme is straightforward. Before iterating, we can first determine the spectral shape function. In Section 3 our Fourier analyses showed that for every test case, the maximum eigenvalue occurred at the Fourier flat mode ($\lambda = 0$). One accelerated iteration begins with an iteration sweep on the fine-grid using (53a) and (53b). The residual terms are calculated using the latest scalar flux solutions in (63), and are then used as a source in the coarse-grid equation (62). This "effectively-mixed" transport equation is solved for the corrections to the effective scalar flux. We project the corrections back onto the fine-grid through the spectral shape function, and add the estimates to the scalar flux solutions to update the accelerated scalar fluxes:

$$\phi_{(1,2)}^{(\ell+1)}(x) = \phi_{(1,2)}^{(\ell+1/2)}(x) + \int_{-1}^{1} \Upsilon_{eff}^{(\ell+1/2)}(x,\mu')\, \xi_{(1,2)}(\mu') d\mu' \,. \tag{65}$$

This describes one accelerated iteration, and we continue this process until the scalar flux solutions converge within a given tolerance value.

4.3 Analysis

Upon observation, we note that our two-grid acceleration procedure now employs three iteration levels: (ℓ), $(\ell + 1/2)$, and $(\ell + 1)$. Therefore, we define Fourier ansatz sets that are similar in form to (39)

$$p_{(1,2)}\epsilon_{(1,2)}^{(\ell,\ell+1)}(x,\mu) \;\cong\; \omega^{(\ell,\ell+1)}\xi_{(1,2)}(\mu)\, e^{i\lambda x} \tag{66a}$$

$$p_{(1,2)}\epsilon_{(1,2)}^{(\ell+1/2)}(x,\mu) \;\cong\; \omega^{(\ell)}\Psi_{(1,2)}(\mu)\, e^{i\lambda x} \tag{66b}$$

$$\Upsilon_{eff}^{(\ell+1/2)}(x,\mu) \;\cong\; \omega^{(\ell)}\xi_{eff}(\mu)\, e^{i\lambda x}\,, \tag{66c}$$

where we can further integrate each angularly-dependent eigenvector over all angles

to calculate scalar components

$$E_{(1,2)} = \int_{-1}^{1} \xi_{(1,2)}(\mu')\, d\mu' \tag{67a}$$

$$\Phi_{(1,2)} = \int_{-1}^{1} \Psi_{(1,2)}(\mu')\, d\mu' \tag{67b}$$

$$\begin{aligned} E_{eff} &= \int_{-1}^{1} \left[\xi_1(\mu') + \xi_2(\mu')\right] d\mu' \\ &= \int_{-1}^{1} \xi_{eff}(\mu')\, d\mu' . \end{aligned} \tag{67c}$$

We begin the Fourier analysis by substituting the ansatz into the fine-grid system of (56a) and (56b) in a similar fashion as described in Section 3.2.3.

$$\left[\Psi_1(\mu)\left(i\mu\lambda + \sigma_1 + \frac{|\mu|}{\Lambda_1}\right) - \frac{|\mu|}{\Lambda_2}\Psi_2(\mu)\right] = \frac{\sigma_{s1}}{2}E_1 \tag{68a}$$

$$\left[\Psi_2(\mu)\left(i\mu\lambda + \sigma_2 + \frac{|\mu|}{\Lambda_2}\right) - \frac{|\mu|}{\Lambda_1}\Psi_1(\mu)\right] = \frac{\sigma_{s2}}{2}E_2 . \tag{68b}$$

This system can be rearranged in terms of $\Psi(\mu)$ in matrix form,

$$\begin{bmatrix} \Psi_1(\mu) \\ \Psi_2(\mu) \end{bmatrix} = \begin{bmatrix} i\mu\lambda + \sigma_1 + \dfrac{|\mu|}{\Lambda_1} & -\dfrac{|\mu|}{\Lambda_2} \\ -\dfrac{|\mu|}{\Lambda_1} & i\mu\lambda + \sigma_2 + \dfrac{|\mu|}{\Lambda_2} \end{bmatrix}^{-1} \begin{bmatrix} \dfrac{\sigma_{s1}}{2} & 0 \\ 0 & \dfrac{\sigma_{s2}}{2} \end{bmatrix} \begin{bmatrix} E_1 \\ E_2 \end{bmatrix} . \tag{69}$$

Integrating the solutions over all angles yields scalar quantities such that the system relates the error in the scalar fluxes at iteration level $(\ell+1/2)$ to the scalar flux errors at level (ℓ). This system can be expressed as

$$\mathbf{\Phi} = \mathbf{S}^{-1}\boldsymbol{\sigma}_s\mathbf{E}, \tag{70}$$

where,

$\mathbf{\Phi}$ = scalar error vector from $(\ell + 1/2)$,

$\mathbf{S}$ = streaming, collision and coupling matrix,

$\boldsymbol{\sigma_s}$= scattering matrix, and

$\mathbf{E}$ = scalar error vector from (ℓ).

Next, we use (62) to derive the Fourier system corresponding to the coarse-grid operator:

$$\mu\frac{\partial}{\partial x}\Upsilon_{eff}^{(\ell+1/2)}(x,\mu)+\sigma_{eff}(\mu)\Upsilon_{eff}^{(\ell+1/2)}(x,\mu)-\frac{1}{2}\int_{-1}^{1}\sigma_{s,eff}(\mu')\Upsilon_{eff}^{(\ell+1/2)}(x,\mu)d\mu'$$

$$=\frac{1}{2}\sigma_{s1}p_1\left[\phi_1^{(\ell+1/2)}(x)-\phi_1^{(\ell)}(x)\right]+\frac{1}{2}\sigma_{s2}p_2\left[\phi_2^{(\ell+1/2)}(x)-\phi_2^{(\ell)}(x)\right]\ . \quad (71)$$

Using the ansatz sets, we rewrite (71),

$$\mu\frac{\partial}{\partial x}\omega^{(\ell)}\xi_{eff}\left(\mu\right)e^{i\lambda x}+\sigma_{eff}(\mu)\omega^{(\ell)}\xi_{eff}\left(\mu\right)e^{i\lambda x}$$

$$-\frac{1}{2}\int_{-1}^{1}\sigma_{s,eff}(\mu')\omega^{(\ell)}\xi_{eff}\left(\mu'\right)e^{i\lambda x}d\mu'$$

$$=\frac{1}{2}\left[\omega^{(\ell)}\sigma_{s1}\Phi_1e^{i\lambda x}+\omega^{(\ell)}\sigma_{s2}\Phi_2e^{i\lambda x}\right]$$

$$-\frac{1}{2}\left[\omega^{(\ell)}\sigma_{s1}E_1e^{i\lambda x}+\omega^{(\ell)}\sigma_{s2}E_2e^{i\lambda x}\right]\ , \quad (72)$$

but cancelling like-terms and performing the spatial derivative, we arrive at the eigen-system for the coarse-grid:

$$\xi_{eff}\left(\mu\right)\left[i\mu\lambda+\sigma_{eff}(\mu)\right]-\frac{1}{2}\int_{-1}^{1}\sigma_{s,eff}(\mu')\xi_{eff}\left(\mu'\right)d\mu'$$

$$=\frac{1}{2}\left[\sigma_{s1}\Phi_1+\sigma_{s2}\Phi_2\right]-\frac{1}{2}\left[\sigma_{s1}E_1+\sigma_{s2}E_2\right]\ . \quad (73)$$

Alternatively, in matrix form,

$$\boldsymbol{\xi}_{\mathbf{eff}}=\mathbf{S}_{\mathbf{eff}}{}^{-1}\boldsymbol{\sigma_s}\left(\boldsymbol{\Phi}-\mathbf{E}\right)\ , \quad (74)$$

where,

$\boldsymbol{\xi}_{\mathbf{eff}}$ = effective angular flux error vector, and

$\mathbf{S}_{\mathbf{eff}}$ = streaming, effective collision and ordinate weight matrix.

Finally, the error estimate in the accelerated iterate is given by (65) for which the respective Fourier ansatz are substituted

$$\omega^{(\ell+1)} E_1 e^{i\lambda x} = \omega^{(\ell)} \Phi_1 e^{i\lambda x} + \omega^{(\ell)} \int_{-1}^{1} \xi_{eff}(\mu)\, e^{i\lambda x} \xi_1(\mu)\, d\mu' \tag{75a}$$

$$\omega^{(\ell+1)} E_2 e^{i\lambda x} = \omega^{(\ell)} \Phi_2 e^{i\lambda x} + \omega^{(\ell)} \int_{-1}^{1} \xi_{eff}(\mu)\, e^{i\lambda x} \xi_2(\mu)\, d\mu' . \tag{75b}$$

Approximating the integral using the Gauss-Legendre quadrature set, this coupled system simplifies to

$$\omega E_1 = \Phi_1 + \sum_{m=1}^{N} \mathrm{w}_m \xi_{eff}(\mu_m)\, \xi_1(\mu_m) \tag{76a}$$

$$\omega E_2 = \Phi_2 + \sum_{m=1}^{N} \mathrm{w}_m \xi_{eff}(\mu_m)\, \xi_2(\mu_m) , \tag{76b}$$

where the ordinate weights are stored in a vector, $\mathbf{w}$. This update system of equations can be written in the matrix form

$$\omega\, \mathbf{E} = \boldsymbol{\Phi} + \boldsymbol{\xi}\, \mathbf{w}\, \boldsymbol{\xi}_{\mathbf{eff}} . \tag{77}$$

However, substituting the relationships from the fine-grid, (70), and the coarse-grid, (74), into (77) yields the governing eigenvalue problem describing the two-grid acceleration scheme

$$\omega\, \mathbf{E} = \left[\mathbf{S}^{-1}\, \boldsymbol{\sigma} + \boldsymbol{\xi}\, \mathbf{w}\, {\mathbf{S}_{\mathbf{eff}}}^{-1}\, \boldsymbol{\sigma}\, \left(\mathbf{S}^{-1}\, \boldsymbol{\sigma} - \mathbf{I}\right)\right] \mathbf{E} . \tag{78}$$

4.4 Results

Using the same material data from the Adams et al. [MAda 89] benchmark cases listed in Table 1, we again perform our Fourier analyses of the two-grid acceleration scheme through analytic and discretized calculations.

4.4.1 Analytic Results

The analytic MAPLE-V analyses were performed on Sun Ultra-10 workstations at Oregon State University. The two-grid acceleration technique developed by Adams and Morel proved to attenuate the spectral radius of the unaccelerated system. From Section 3, we already know that our *largest* unaccelerated eigenvalues (spectral radii) occur at the Fourier flat mode. Table 3 compares the eigenvalues at $\lambda = 0$ with and without the acceleration.

Table 3: Eigenvalues at $\lambda = 0$ with and without acceleration

case #:	unaccelerated $\|\omega\|$:	accelerated $\|\omega\|$:
1	0.924619	0.003298
2	0.246187	0.000006
3	0.900000	0.153725
4	0.968480	0.044110
5	0.684799	0.000003
6	0.900000	0.587951
7	0.991910	0.001008
8	0.191045	0.000011
9	0.900000	0.164660

In the multigroup S_N problems with upscattering, Adams and Morel found that the *accelerated* spectral radius was equal to the *second-largest* eigenvalue. Although Adams and Morel derived an exact one-group diffusion equation for the Fourier mode corresponding to the unaccelerated spectral radius, the acceleration procedure is not guaranteed to have an impact on the remaining error modes. Furthermore the effectiveness of the two-grid method showed a dependence on the material properties, specifically, the cross-sections. While we chose to use an exact "effectively-mixed" transport equation, this characteristic cannot be dismissed. In fact, the material coupling (characterized by the transition lengths, Λ) also influences the behavior of the acceleration scheme when applied to the coupled stochastic mixture system.

Figures 12 through 20 show the behavior of the two-grid acceleration scheme versus the respective unaccelerated system at each Fourier mode. We note that for each of the nine test cases, the accelerated eigenvalues are always less than the unaccelerated eigenvalues. For cases where the optically-thick material is purely-absorbing (cases 2, 5, and 8), the two-grid acceleration scheme not only attenuates the unaccelerated eigenvalues at $\lambda = 0$, but the eigenvalues at intermediate and higher modal frequencies as well. Unlike the multigroup, upscattering problems treated by Adams and Morel, the spectral radius of our acceleration scheme does not occur at the same Fourier mode. While our unaccelerated spectral radii occur at $\lambda = 0$, the accelerated spectral radii are found at intermediate and higher Fourier modes.

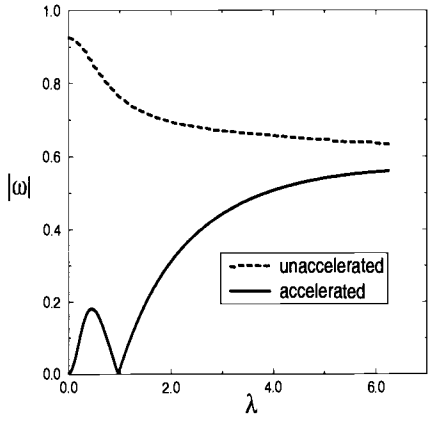

Fig. 12: Eigenvalues of the acceleration scheme (case 1)

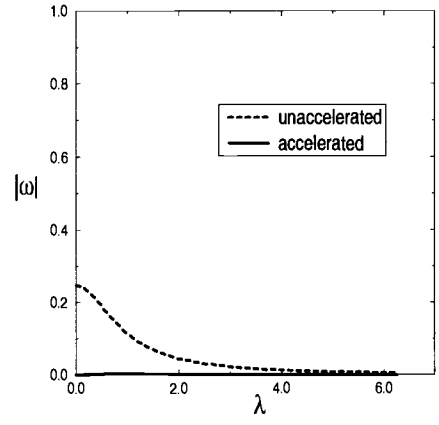

Fig. 13: Eigenvalues of the acceleration scheme (case 2)

4.4.2 Discretized Results

We verify the analytic results of the two-grid acceleration scheme with discretized-in-space calculations from a FORTRAN-90 implementation code. The same assumptions from the unaccelerated discretized-in-space analysis (tolerance, random initial scalar flux guesses, maximum zone size, etc.) were applied, and we also discretized the spatial variable, x, using the diamond-difference method.

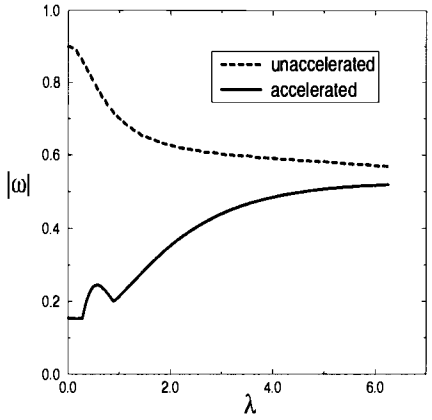

Fig. 14: Eigenvalues of the acceleration scheme (case 3)

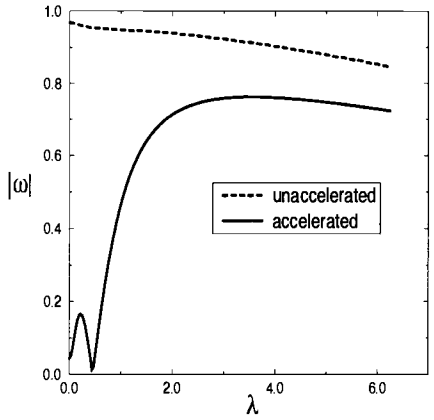

Fig. 15: Eigenvalues of the acceleration scheme (case 4)

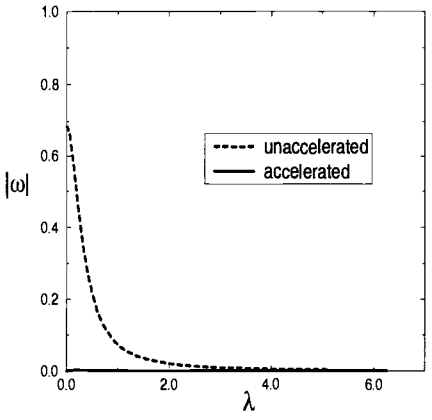

Fig. 16: Eigenvalues of the acceleration scheme (case 5)

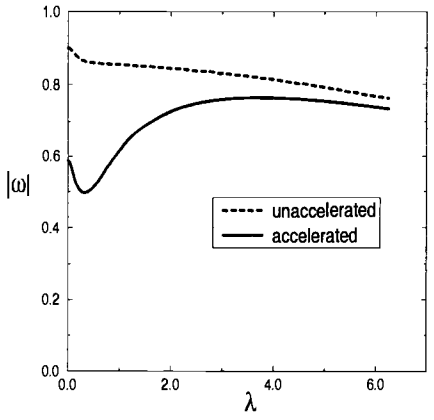

Fig. 17: Eigenvalues of the acceleration scheme (case 6)

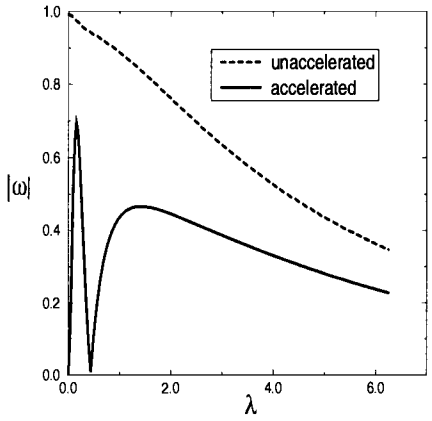

Fig. 18: Eigenvalues of the acceleration scheme (case 7)

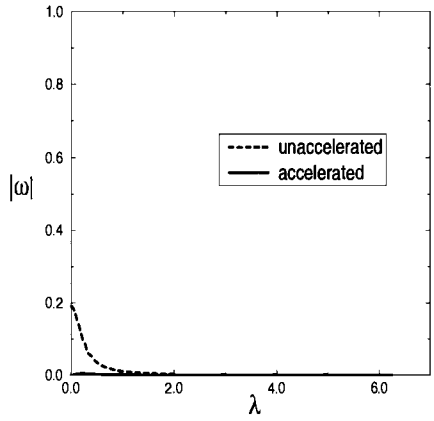

Fig. 19: Eigenvalues of the acceleration scheme (case 8)

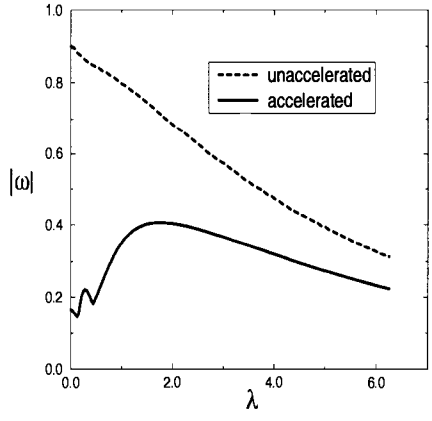

Fig. 20: Eigenvalues of the acceleration scheme (case 9)

Already knowing the Fourier mode where the unaccelerated spectral radii occur allows us to first determine the spectral shape function, ξ from (45). We then begin the iteration process by sweeping in both directions on the fine-grid with explicit equations similar to (53a) and (53b). However, in the accelerated case, we denote the resulting angular flux solutions from the fine-grid with iteration level $(\ell + 1/2)$

$$
\begin{aligned}
& p_1\psi_{1,k+1/2,m}^{(\ell+1/2)} = \\
& \left\{ \left[\mu_m \Delta x \frac{|\mu_m|}{\Lambda_2} \right] p_2\psi_{2,k-1/2,m}^{(\ell+1/2)} + \left[\mu_m + \frac{\Delta x}{2}\hat{\sigma}_{2,m} \right] \Delta x p_1 Q_{1,k}^{(\ell)} + \frac{\Delta x_k^2}{2} \frac{|\mu_m|}{\Lambda_2} p_2 Q_{2,k}^{(\ell)} \right. \\
& \left. - \left(\left[\mu_m + \frac{\Delta x}{2}\hat{\sigma}_{2,m} \right] \left[-\mu_m + \frac{\Delta x}{2}\hat{\sigma}_{1,m} \right] - \left(\frac{\Delta x}{2} \right)^2 \frac{\mu_m^2}{\Lambda_1\Lambda_2} \right) p_1\psi_{1,k-1/2,m}^{(\ell+1/2)} \right\} \\
& \Bigg/ \left\{ \left[\mu_m + \frac{\Delta x}{2}\hat{\sigma}_{2,m} \right] \left[\mu_m + \frac{\Delta x}{2}\hat{\sigma}_{1,m} \right] - \left(\frac{\Delta x}{2} \right)^2 \frac{\mu_m^2}{\Lambda_1\Lambda_2} \right\}, \quad \mu_m > 0
\end{aligned}
\tag{79a}
$$

$$
\begin{aligned}
& p_2\psi_{2,k+1/2,m}^{(\ell+1/2)} = \\
& \left\{ \left[\mu_m \Delta x \frac{|\mu_m|}{\Lambda_1} \right] p_1\psi_{1,k-1/2,m}^{(\ell+1/2)} + \left[\mu_m + \frac{\Delta x}{2}\hat{\sigma}_{1,m} \right] \Delta x p_2 Q_{2,k}^{(\ell)} + \frac{\Delta x^2}{2} \frac{|\mu_m|}{\Lambda_1} p_1 Q_{1,k}^{(\ell)} \right. \\
& \left. - \left(\left[\mu_m + \frac{\Delta x}{2}\hat{\sigma}_{1,m} \right] \left[-\mu_m + \frac{\Delta x}{2}\hat{\sigma}_{2,m} \right] - \left(\frac{\Delta x}{2} \right)^2 \frac{\mu_m^2}{\Lambda_1\Lambda_2} \right) p_2\psi_{2,k-1/2,m}^{(\ell+1/2)} \right\} \\
& \Bigg/ \left\{ \left[\mu_m + \frac{\Delta x}{2}\hat{\sigma}_{2,m} \right] \left[\mu_m + \frac{\Delta x}{2}\hat{\sigma}_{1,m} \right] - \left(\frac{\Delta x}{2} \right)^2 \frac{\mu_m^2}{\Lambda_1\Lambda_2} \right\}, \quad \mu_m > 0
\end{aligned}
\tag{79b}
$$

By integrating over all angles with (46) we compute the corresponding scalar fluxes at $(\ell + 1/2)$.

The next task is to solve the "effectively-mixed" transport equation (62) using the previous and most-recent scalar fluxes, (ℓ) and $(\ell+1/2)$, respectively, to calculate the residual terms. In order to be consistent with the fine-grid solution, we discretize the equation with the diamond-difference method. Integrating (62) between zone edges $x_{k-1/2}$ and $x_{k+1/2}$, and then substituting the diamond-difference relationship (48)

yields

$$\frac{\mu_m}{\Delta x}\left[\Upsilon^{(\ell+1/2)}_{eff,k+1/2,m} - \Upsilon^{(\ell+1/2)}_{eff,k-1/2,m}\right]$$

$$+\frac{1}{2}\sigma_{eff,m}\left[\Upsilon^{(\ell+1/2)}_{eff,k-1/2,m} + \Upsilon^{(\ell+1/2)}_{eff,k+1/2,m}\right]$$

$$= \frac{1}{2}\sum_{m=1}^{N} \mathrm{w}_m \sigma_{s,eff,m}\Upsilon^{(\ell)}_{eff,k,m} + \frac{R^{(\ell+1/2)}_{1,k}}{2} + \frac{R^{(\ell+1/2)}_{2,k}}{2}. \quad (80)$$

Note that the angular flux error estimate within the integral has been lagged to the previous iteration level (ℓ) so that we can employ the source iteration technique, i.e., we guess this term, and then iterate until convergence. Solving for the updated exiting angular flux errors, we obtain an explicit equation for one directional sweep

$$\Upsilon^{(\ell+1/2)}_{eff,k+1/2,m} =$$

$$\frac{2\Delta x Q^{(\ell)}_{eff,k} + 2\mu_m \Upsilon^{(\ell+1/2)}_{eff,k-1/2,m} - \sigma_{eff,m}\Delta x \Upsilon^{(\ell+1/2)}_{eff,k-1/2,m}}{2\mu_m + \sigma_{eff,m}\Delta x}, \quad \mu_m > 0 \quad (81)$$

where for convenience, we have defined

$$Q^{(\ell)}_{eff,k} = \frac{1}{2}\sum_{m=1}^{N} \mathrm{w}_m \sigma_{s,eff,m}\Upsilon^{(\ell)}_{eff,k,m} + \frac{R^{(\ell+1/2)}_{1,k}}{2} + \frac{R^{(\ell+1/2)}_{2,k}}{2}. \quad (82)$$

To complete one accelerated iteration, the coarse-grid angular flux error estimate is weighted by the spectral shape function from the fine-grid operator, integrated over all angles, and finally added to the scalar flux solutions from the fine-grid as described by (65).

$$\phi^{(\ell+1)}_{(1,2),k} = \phi^{(\ell+1/2)}_{(1,2),k} + \sum_{m=1}^{N} \Upsilon^{(\ell+1/2)}_{eff,k,m}\, \xi_{(1,2),m}\, \mathrm{w}_m \quad (83)$$

The FORTRAN-90 acceleration code was run with the material data from the nine test cases, and executed on the Lawrence Livermore National Laboratory systems mentioned in Section 3.4.2. Table 4 compares the unaccelerated theoretical spectral

Table 4: Performance of the accelerated, fully-implicit iteration scheme

case #:	unaccelerated theoretical $\lvert\rho\rvert$:	accelerated theoretical $\lvert\rho\rvert$:	accelerated computational $\lvert\rho\rvert$:	relative error [%]:
1	0.924619	0.560205	0.54591	-2.55174
2	0.246187	0.002989	0.00237	-20.70927
3	0.900000	0.518922	0.49588	-4.44036
4	0.968480	0.762446	0.75921	-0.42442
5	0.684799	0.002635	0.00171	-35.10436
6	0.900000	0.763959	0.75565	-1.08762
7	0.991910	0.695584	0.68711	-1.21826
8	0.191045	0.004105	0.00312	-23.99513
9	0.900000	0.405868	0.38535	-5.05534

radii to the accelerated theoretical and computational spectral radii. The latter were calculated for each iteration according to (55).

For all nine test cases, the accelerated computational spectral radii agree (within precision and tolerance) with the expected values from the theoretical analyses. However, the effects of machine precision and round-off error become more prominent, most notably in cases 2, 5, and 8 where the optically-thick material is purely-absorbing. For these cases, the spectral radii are very small, and could be dependent on machine type. Also, as in Section 3.4.2, the computational results are less than the corresponding theoretical results as a consequence of truncating an infinite slab.

Nonetheless, we observe accelerated spectral radii that are, in some cases, significantly less than the unaccelerated results. For a simple illustration of the acceleration, we can predict the number of iterations, Z, required to reduce the error by a certain factor, say 10^{-5}, such that

$$\rho^Z = 10^{-5} \tag{84}$$

Therefore, from case 1, the unaccelerated system would require approximately

$$Z(unaccelerated) = \frac{\log 10^{-5}}{\log 0.924619} \approx 147 \text{ iterations},$$

while the two-grid accelerated system would require only

$$Z(accelerated) = \frac{\log 10^{-5}}{\log 0.560205} \approx 20 \text{ iterations!}$$

We immediately see that this two-grid acceleration scheme can substantially reduce the required number of iterations to converge to a solution. Theoretically, for the purely-absorbing, optically-thick cases, the acceleration scheme should converge after a single iteration. However, we must note that the analyses covered in Sections 4.3 through 4.4 do not address the convergence of the coarse-grid operator. For the problems where the effective scattering ratios are close to or equal to unity, the coarse-grid transport operator can converge very slowly, thereby hampering the efficiency of the two-grid method. Another acceleration scheme, such as the robust diffusion synthetic acceleration (DSA) technique, could be used to to solve the coarse-grid operator, and should eliminate this problem. This is discussed in Section 5.

5 COARSE-GRID DIFFUSION SYNTHETIC ACCELERATION

In our previous analysis of the two-grid acceleration scheme, we neglected the convergence of the coarse-grid solution. However, since the low-order operator represented by (62) itself is a transport calculation, it may also converge slowly for highly-scattering media if solved with Source Iteration. This effect would prove detrimental to the efficiency of the two-grid acceleration scheme. Therefore, the coarse-grid also requires an acceleration scheme.

Similar to our two-grid method, the popular technique known as "Diffusion Synthetic Acceleration," or "DSA," employs a low-order approximation to the transport operator. In this case, however, it is in the form of a diffusion approximation, and its solution provides a correction factor to update the transport sweep calculation. Since we choose to solve the coarse-grid with Source Iteration, one coarse-grid iteration now requires a transport sweep *and* a diffusion calculation. The additional computational cost of DSA is justified only if it results in significantly fewer total iterations.

In this section, we begin with a derivation of the acceleration equations, and we later employ Larsen's 4-step method [Lar 82] to formulate the discretized diffusion equations for the coarse-grid acceleration. We then present the Fourier analysis and results of applying DSA.

5.1 Derivation of the Diffusion Synthetic Acceleration Equations

For the DSA technique, we derive a diffusion approximation to the low-order transport equation. The solution of this diffusion approximation is easily obtained and is used as an exact correction to the Source Iteration flux. To derive the DSA system of equations, we apply Larsen's 4-step procedure:

1. Write the transport equation for the exact correction to the Source Iteration solution of (62).

2. Take the 0th angular moment of the transport equation from Step 1.

3. Take the 1st angular moment of the transport equation from Step 1.

4. Collapse the two equations from Steps 2 and 3 into a diffusion approximation to (62).

We begin with the low-order transport Source Iteration equation [(62)]:

$$\mu\frac{\partial}{\partial x}\Upsilon_{eff}^{(\alpha+1/2)}(x,\mu)+\sigma_{eff}(\mu)\Upsilon_{eff}^{(\alpha+1/2)}(x,\mu)$$

$$=\frac{1}{2}\int_{-1}^{1}\sigma_{s,eff}(\mu')\Upsilon_{eff}^{(\alpha)}(x,\mu')d\mu'+\frac{R_1^{(\ell+1/2)}(x)}{2}+\frac{R_2^{(\ell+1/2)}(x)}{2},$$

where α denotes the iteration level(s) for the low-order transport Source Iteration, and the residual terms are already known from the two-grid calculation. Next, recall its corresponding exact equation

$$\mu\frac{\partial}{\partial x}\Upsilon_{eff}(x,\mu)+\sigma_{eff}(\mu)\Upsilon_{eff}(x,\mu)$$

$$=\frac{1}{2}\int_{-1}^{1}\sigma_{s,eff}(\mu')\Upsilon_{eff}(x,\mu')d\mu'+\frac{R_1^{(\ell+1/2)}(x)}{2}+\frac{R_2^{(\ell+1/2)}(x)}{2}. \qquad (85)$$

Subtracting (62) from (85) we obtain another system of equations for iteration errors:

$$\mu\frac{\partial}{\partial x}f^{(\alpha+1/2)}(x,\mu)+\sigma_{eff}(\mu)f^{(\alpha+1/2)}(x,\mu)$$

$$=\frac{1}{2}\int_{-1}^{1}\sigma_{s,eff}(\mu')\Upsilon_{eff}(x,\mu')d\mu'-\frac{1}{2}\int_{-1}^{1}\sigma_{s,eff}(\mu')\Upsilon_{eff}^{(\alpha)}(x,\mu')d\mu', \qquad (86)$$

where we have defined

$$f^{(\alpha+1/2)}(x,\mu)=\Upsilon_{eff}(x,\mu)-\Upsilon_{eff}^{(\alpha+1/2)}(x,\mu). \qquad (87)$$

Equation (86) can be written as

$$\mu\frac{\partial}{\partial x}f^{(\alpha+1/2)}(x,\mu)+\sigma_{eff}(\mu)f^{(\alpha+1/2)}(x,\mu)-\frac{1}{2}\int_{-1}^{1}\sigma_{s,eff}(\mu')f^{(\alpha+1/2)}(x,\mu')d\mu'$$

$$=\frac{1}{2}\int_{-1}^{1}\sigma_{s,eff}(\mu')\Upsilon_{eff}^{(\alpha+1/2)}(x,\mu')d\mu'-\frac{1}{2}\int_{-1}^{1}\sigma_{s,eff}(\mu')\Upsilon_{eff}^{(\alpha)}(x,\mu')d\mu'\,. \quad (88)$$

We approximate f with a two-term Legendre polynomial expansion in angle:

$$f^{(\alpha+1/2)}(x,\mu)\cong\frac{1}{2}F^{(\alpha+1/2)}(x)+\frac{3}{2}\mu J^{(\alpha+1/2)}(x)\,, \quad (89)$$

such that F and J satisfy

$$F^{(\alpha+1/2)}(x) = \int_{-1}^{1}f^{(\alpha+1/2)}(x,\mu)d\mu'\,, \quad (90a)$$

$$J^{(\alpha+1/2)}(x) = \int_{-1}^{1}\mu f^{(\alpha+1/2)}(x,\mu)d\mu'\,. \quad (90b)$$

Equation (88) then becomes:

$$\mu\frac{\partial}{\partial x}\left[\frac{1}{2}F^{(\alpha+1/2)}(x)+\frac{3}{2}\mu J^{(\alpha+1/2)}(x)\right]+\sigma_{eff}(\mu)\left[\frac{1}{2}F^{(\alpha+1/2)}(x)+\frac{3}{2}\mu J^{(\alpha+1/2)}(x)\right]$$

$$-\frac{1}{2}\int_{-1}^{1}\sigma_{s,eff}(\mu')\left[\frac{1}{2}F^{(\alpha+1/2)}(x)+\frac{3}{2}\mu' J^{(\alpha+1/2)}(x)\right]d\mu'$$

$$=\frac{1}{2}\int_{-1}^{1}\sigma_{s,eff}(\mu')\Upsilon_{eff}^{(\alpha+1/2)}(x,\mu')d\mu'-\frac{1}{2}\int_{-1}^{1}\sigma_{s,eff}(\mu')\Upsilon_{eff}^{(\alpha)}(x,\mu')d\mu'\,. \quad (91)$$

In deriving the diffusion approximation to (88), we first write its 0th angular moment of (91):

$$\frac{\partial}{\partial x}J^{(\alpha+1/2)}(x)+\sigma_{a,eff,0}F^{(\alpha+1/2)}(x)$$

$$=\int_{-1}^{1}\sigma_{s,eff}(\mu')\Upsilon_{eff}^{(\alpha+1/2)}(x,\mu')d\mu'-\int_{-1}^{1}\sigma_{s,eff}(\mu')\Upsilon_{eff}^{(\alpha)}(x,\mu')d\mu'\,, \quad (92)$$

where,

$$\sigma_{eff,0}=\frac{\displaystyle\int_{-1}^{1}\sigma_{eff}(\mu')d\mu'}{\displaystyle\int_{-1}^{1}d\mu'} \quad \text{and} \quad \sigma_{s,eff,0}=\frac{\displaystyle\int_{-1}^{1}\sigma_{s,eff}(\mu')d\mu'}{\displaystyle\int_{-1}^{1}d\mu'}\,. \quad (93)$$

We also define an "effective" absorption cross-section:

$$\sigma_{a,eff,0} = \sigma_{eff,0} - \sigma_{s,eff,0} \,. \tag{94}$$

Taking the 1st angular moment of (91), we obtain:

$$\frac{1}{3}\frac{\partial}{\partial x}F^{(\alpha+1/2)}(x) + \sigma_{eff,2}J^{(\alpha+1/2)}(x) = 0\,,$$

or,

$$J^{(\alpha+1/2)}(x) = -\frac{1}{3\sigma_{eff,2}}\frac{\partial}{\partial x}F^{(\alpha+1/2)}(x)\,. \tag{95}$$

In this instance, we have defined

$$\sigma_{eff,2} = \frac{3\int_{-1}^{1}\mu'^{\,2}\sigma_{eff}(\mu')d\mu'}{\int_{-1}^{1}d\mu'}\,. \tag{96}$$

By substituting (95) into (92) we arrive at the second equation, which is simply a diffusion equation:

$$-\frac{\partial}{\partial x}\frac{1}{3\sigma_{eff,2}}\frac{\partial}{\partial x}F^{(\alpha+1/2)}(x) + \sigma_{a,eff,0}F^{(\alpha+1/2)}(x)$$

$$= \int_{-1}^{1}\sigma_{s,eff}(\mu')\Upsilon_{eff}^{(\alpha+1/2)}(x,\mu')d\mu' - \int_{-1}^{1}\sigma_{s,eff}(\mu')\Upsilon_{eff}^{(\alpha)}(x,\mu')d\mu'\,. \tag{97}$$

F is an additive correction to the Source Iteration intensity. Applying this correction gives the new estimate of the scattering reaction rate:

$$\int_{-1}^{1}\sigma_{s,eff}(\mu')\Upsilon_{eff}^{(\alpha+1)}(x,\mu')d\mu'$$

$$= \int_{-1}^{1}\sigma_{s,eff}(\mu')\Upsilon_{eff}^{(\alpha+1/2)}(x,\mu')d\mu' + \frac{1}{2}F^{(\alpha+1/2)}(x)\int_{-1}^{1}\sigma_{s,eff}(\mu')d\mu'\,. \tag{98}$$

To summarize the coarse-grid DSA procedure for a given two-grid iteration, we begin solving the coarse-grid transport equation of (62) using the standard Source Iteration scheme with an initial guess for $\Upsilon_{eff}^{(\alpha)}$. The residual terms, $R_{(1,2)}$, act as source

terms, and are already known from the two-grid calculation of (63). An updated value for $\Upsilon_{eff}^{(\alpha+1/2)}$ is then applied in (97) to determine correction factors, $F^{(\alpha+1/2)}$, that in turn are used to update $\Upsilon_{eff}^{(\alpha+1)}$. The iteration process is repeated until Υ_{eff} is converged within a given tolerance.

5.2 Analysis

The Fourier analysis of the coarse-grid DSA begins with (86).

$$\mu\frac{\partial}{\partial x}f^{(\alpha+1/2)}(x,\mu)+\sigma_{eff}(\mu)f^{(\alpha+1/2)}(x,\mu)=\frac{1}{2}\int_{-1}^{1}\sigma_{s,eff}(\mu')f^{(\alpha)}(x,\mu')d\mu'\,. \tag{99}$$

As in our previous analyses of Sections 3 and 4, we define the errors, f, as

$$f^{(\alpha,\alpha+1/2)}(x,\mu)=\Upsilon_{eff}(x,\mu)-\Upsilon_{eff}^{(\alpha,\alpha+1/2)}(x,\mu)\,. \tag{100}$$

We also rewrite the remaining two acceleration equations with consistent notation:

$$\begin{aligned}&-\frac{\partial}{\partial x}\frac{1}{3\sigma_{eff,2}}\frac{\partial}{\partial x}F^{(\alpha+1/2)}(x)+\sigma_{a,eff,0}F^{(\alpha+1/2)}(x)\\&\quad=\int_{-1}^{1}\sigma_{s,eff}(\mu')f^{(\alpha+1/2)}(x,\mu')d\mu'-\int_{-1}^{1}\sigma_{s,eff}(\mu')f^{(\alpha)}(x,\mu')d\mu'\,,\end{aligned} \tag{101}$$

and

$$\begin{aligned}&\int_{-1}^{1}\sigma_{s,eff}(\mu')f^{(\alpha+1)}(x,\mu')d\mu'\\&\quad=\int_{-1}^{1}\sigma_{s,eff}(\mu')f^{(\alpha+1/2)}(x,\mu')d\mu'+\frac{1}{2}F^{(\alpha+1/2)}(x)\int_{-1}^{1}\sigma_{s,eff}(\mu')d\mu'\,.\end{aligned} \tag{102}$$

We define the Fourier ansatz

$$f^{(\alpha,\alpha+1)} \cong \omega^{(\alpha,\alpha+1)}a\,(\mu)\,e^{i\lambda x} \tag{103a}$$

$$f^{(\alpha+1/2)} \cong \omega^{(\alpha)}b\,(\mu)\,e^{i\lambda x} \tag{103b}$$

$$F^{(\alpha+1/2)} \cong \omega^{(\alpha)}Ce^{i\lambda x}\,. \tag{103c}$$

Substituting the ansatz into (99) yields

$$\mu\frac{\partial}{\partial x}\left[\omega^{(\alpha)}b\left(\mu\right)e^{i\lambda x}\right]+\sigma_{eff}(\mu)\left[\omega^{(\alpha)}b\left(\mu\right)e^{i\lambda x}\right]$$

$$=\frac{1}{2}\int_{-1}^{1}\sigma_{s,eff}(\mu')\left[\omega^{(\alpha)}a\left(\mu'\right)e^{i\lambda x}\right]d\mu'. \tag{104}$$

Equation (104) is simplified and solved for $b(\mu)$,

$$b\left(\mu\right)=\frac{\frac{1}{2}\int_{-1}^{1}\sigma_{s,eff}(\mu')a\left(\mu'\right)d\mu'}{i\mu\lambda+\sigma_{eff}\left(\mu\right)}. \tag{105}$$

Likewise, substituting the ansatz into the diffusion approximation of (101) gives

$$-\frac{\partial}{\partial x}\frac{1}{3\sigma_{eff,2}}\frac{\partial}{\partial x}\left[\omega^{(\alpha)}Ce^{i\lambda x}\right]+\sigma_{a,eff,0}\left[\omega^{(\alpha)}Ce^{i\lambda x}\right]$$

$$=\int_{-1}^{1}\sigma_{s,eff}(\mu')\left[\omega^{(\alpha)}b\left(\mu\right)e^{i\lambda x}\right]d\mu'-\int_{-1}^{1}\sigma_{s,eff}(\mu')\left[\omega^{(\alpha)}a\left(\mu'\right)e^{i\lambda x}\right]d\mu', \tag{106}$$

which, after taking the second-order spatial derivative, reduces to

$$\left[\frac{\lambda^2}{3\sigma_{eff,2}}+\sigma_{a,eff,0}\right]C=\int_{-1}^{1}\sigma_{s,eff}(\mu')b\left(\mu\right)d\mu'-\int_{-1}^{1}\sigma_{s,eff}(\mu')a\left(\mu'\right)d\mu'. \tag{107}$$

We rearrange the equation to solve for C:

$$C=D^{-1}\left[\int_{-1}^{1}\sigma_{s,eff}(\mu')b\left(\mu\right)d\mu'-\int_{-1}^{1}\sigma_{s,eff}(\mu')a\left(\mu'\right)d\mu'\right], \tag{108}$$

where

$$D=\left[\frac{\lambda^2}{3\sigma_{eff,2}}+\sigma_{a,eff,0}\right]. \tag{109}$$

Using (105) in (108), we obtain an explicit equation for C:

$$C=D^{-1}\times$$

$$\left[\frac{1}{2}\int_{-1}^{1}\sigma_{s,eff}(\mu')a\left(\mu'\right)d\mu'\cdot\int_{-1}^{1}\frac{\sigma_{s,eff}(\mu)}{i\mu\lambda+\sigma_{eff}\left(\mu\right)}d\mu-\int_{-1}^{1}\sigma_{s,eff}(\mu')a\left(\mu'\right)d\mu'\right],$$

or,

$$C = D^{-1} \int_{-1}^{1} \sigma_{s,eff}(\mu') a(\mu')\, d\mu' \cdot \left[\frac{1}{2} \int_{-1}^{1} \frac{\sigma_{s,eff}(\mu)}{i\mu\lambda + \sigma_{eff}(\mu)} d\mu - 1 \right] . \tag{110}$$

We now substitute the respective ansatz into the update equation of (102):

$$\int_{-1}^{1} \sigma_{s,eff}(\mu') \left[\omega^{(\alpha+1)} a(\mu') e^{i\lambda x} \right] d\mu'$$

$$= \int_{-1}^{1} \sigma_{s,eff}(\mu') \left[\omega^{(\alpha)} b(\mu') e^{i\lambda x} \right] d\mu' + \frac{1}{2} \left[\omega^{(\alpha)} C e^{i\lambda x} \right] \int_{-1}^{1} \sigma_{s,eff}(\mu') d\mu' ,$$

which also simplifies to

$$\omega \int_{-1}^{1} \sigma_{s,eff}(\mu') a(\mu')\, d\mu' = \int_{-1}^{1} \sigma_{s,eff}(\mu') b(\mu')\, d\mu' + \frac{1}{2} C \int_{-1}^{1} \sigma_{s,eff}(\mu') d\mu' . \tag{111}$$

Finally, substitute the relationships for $b(\mu)$ and C into (111),

$$\omega = \frac{1}{2} \int_{-1}^{1} \frac{\sigma_{s,eff}(\mu)}{i\mu\lambda + \sigma_{eff}(\mu)} d\mu + D^{-1} \sigma_{s,eff,0} \left[\frac{1}{2} \int_{-1}^{1} \frac{\sigma_{s,eff}(\mu)}{i\mu\lambda + \sigma_{eff}(\mu)} d\mu - 1 \right] . \tag{112}$$

In writing (112), we must note that we have divided out the term

$$\int_{-1}^{1} \sigma_{s,eff}(\mu') a(\mu')\, d\mu' ,$$

as it is common to each term of the system.

5.3 Results

For the Fourier analysis of the coarse-grid diffusion synthetic acceleration scheme, we again use the material data from the test problems in Adams et al. [MAda 89]. Furthermore, our present analyses were conducted in the same fashion as the analyses of Sections 3 and 4: analytically- and discretized- in space.

5.3.1 *Analytic Fourier Analysis Results*

The analytic calculations were performed on the same Ultra-10 workstations at Oregon State University. We also approximated the integral over angle with the S_4 Gauss-Legendre quadrature set. This aspect is consistent with our previous analyses.

Upon inspection of (112), the Fourier flat mode (λ=0) bounds the eigenvalues such that the $\int_{-1}^{1}[\cdot]$ term obeys:

$$\int_{-1}^{1} \frac{\sigma_{s,eff}(\mu)}{i\mu\lambda + \sigma_{eff}(\mu)} d\mu \xrightarrow{\lambda=0} \int_{-1}^{1} \frac{\sigma_{s,eff}(\mu)}{\sigma_{eff}(\mu)} d\mu .$$

Moreover, since the effective cross-sections are even functions of angle, the coarse-grid diffusion synthetic acceleration produces eigenvalues that are *always* less than 1.0. Figures 21 through 29 illustrate the behavior of the coarse-grid DSA system.

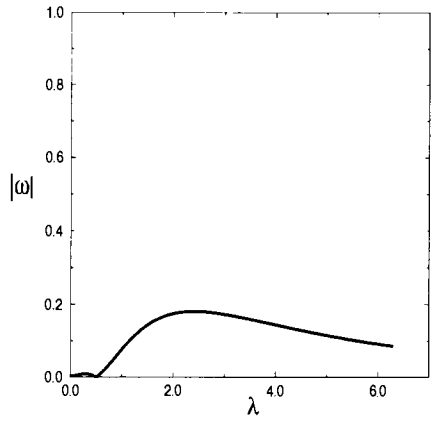

Fig. 21: Eigenvalues of the coarse-grid DSA (case 1)

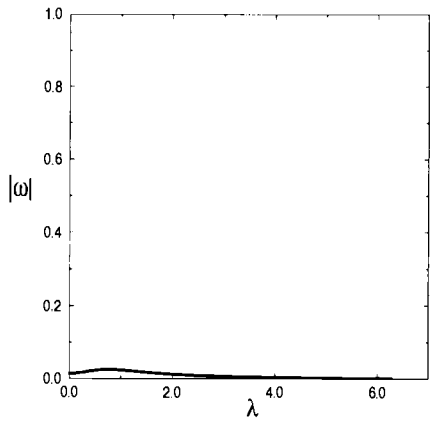

Fig. 22: Eigenvalues of the coarse-grid DSA (case 2)

5.3.2 *Discretized Implementation Results*

We again verify the analytic-in-space results with a discretized-in-space implementation code. The Compaq AlphaServer 4100 Model 5/533 systems at Lawrence Livermore National Laboratory were used to generate the results. For consistency, we approximate an infinite slab with a slab of length 5000 cm, and we also apply the

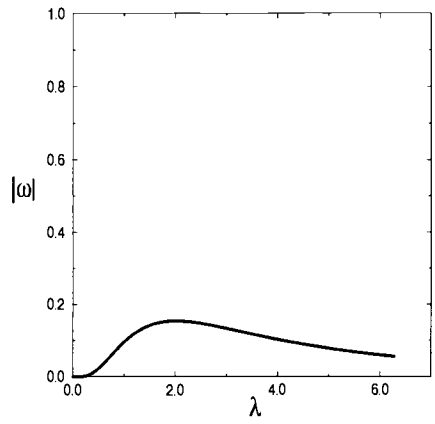

Fig. 23: Eigenvalues of the coarse-grid DSA (case 3)

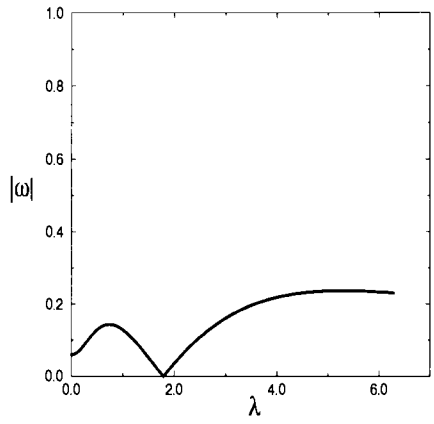

Fig. 24: Eigenvalues of the coarse-grid DSA (case 4)

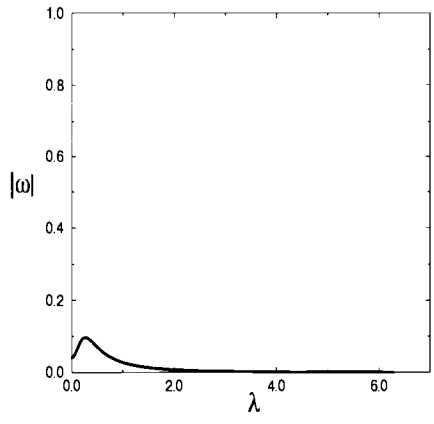

Fig. 25: Eigenvalues of the coarse-grid DSA (case 5)

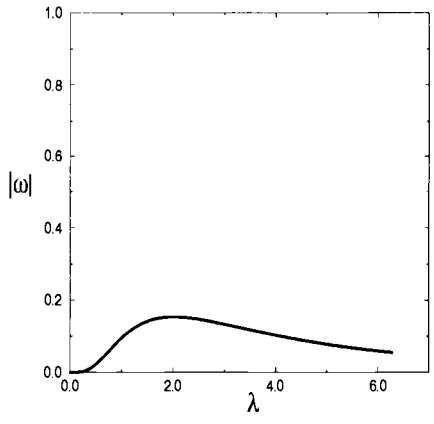

Fig. 26: Eigenvalues of the coarse-grid DSA (case 6)

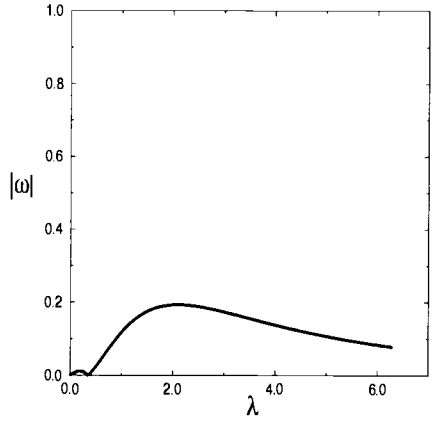

Fig. 27: Eigenvalues of the coarse-grid DSA (case 7)

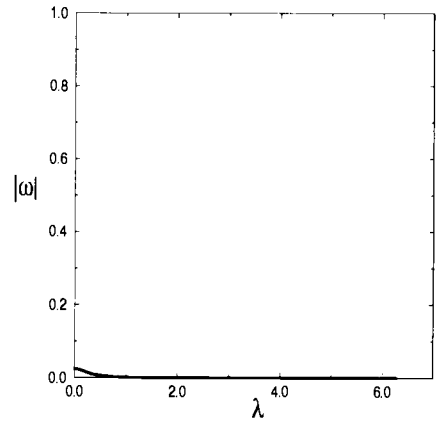

Fig. 28: Eigenvalues of the coarse-grid DSA (case 8)

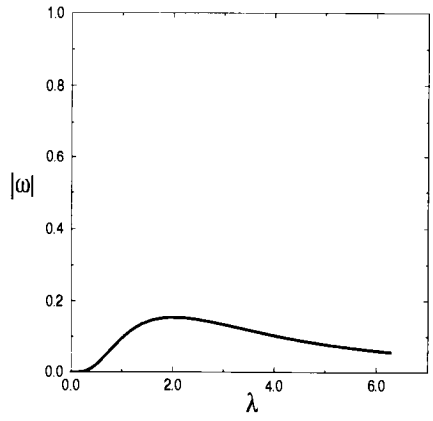

Fig. 29: Eigenvalues of the coarse-grid DSA (case 9)

assumptions of Sections 3.4.2 and 4.4.2 (tolerance, random initial scalar flux guesses, maximum zone size, etc.).

To derive a set of discretized DSA equations, we apply Larsen's 4-step method which we described in Section 5.1. This procedure can be applied to many spatial discretization schemes with symmetric angular quadrature sets. One drawback to the 4-step method is that complicated discretizations yield algebraically complex equations. However, our use of the diamond-difference discretization produces algebraically simple equations.

We now derive the discretized coarse-grid DSA equations according to Larsen's 4-step method. First, recall the coarse-grid S_N equation of (62):

$$\mu_m \frac{\partial}{\partial x} \Upsilon_{eff,k,m}^{(\alpha+1/2)} + \sigma_{eff,m} \Upsilon_{eff,k,m}^{(\alpha+1/2)} = \frac{1}{2} \sum_{m=1}^{N} \mathrm{w}_m \sigma_{s,eff,m} \Upsilon_{eff,k,m}^{(\alpha)} + \frac{1}{2} R_{1,k}^{(\ell+1/2)} + \frac{1}{2} R_{2,k}^{(\ell+1/2)} .$$

Step 1: Obtain an equation for the exact correction. This is represented by the S_N form of (88):

$$\mu_m \frac{\partial}{\partial x} f_{k,m}^{(\alpha+1/2)} + \sigma_{eff,m} f_{k,m}^{(\alpha+1/2)} - \frac{1}{2} \sum_{m=1}^{N} \mathrm{w}_m \sigma_{s,eff,m} f_{k,m}^{(\alpha+1/2)}$$

$$= \frac{1}{2} \sum_{m=1}^{N} \mathrm{w}_m \sigma_{s,eff,m} \Upsilon_{eff,k,m}^{(\alpha+1/2)} - \frac{1}{2} \sum_{m=1}^{N} \mathrm{w}_m \sigma_{s,eff,m} \Upsilon_{eff,k,m}^{(\alpha)} , \qquad (113)$$

where

$$f_{k,m}^{(\alpha+1/2)} = \Upsilon_{eff,k,m} - \Upsilon_{eff,k,m}^{(\alpha+1/2)} ,$$

and according to the diamond-difference discretization, we relate the cell-edges to the cell-midpoints

$$f_{k,m}^{(\alpha+1/2)} = \frac{1}{2} \left[f_{k-1/2,m}^{(\alpha+1/2)} + f_{k+1/2,m}^{(\alpha+1/2)} \right] . \qquad (114)$$

Integrate (113) between zone edges $x_{k-1/2}$ and $x_{k+1/2}$

$$\frac{\mu_m}{\Delta x}\left[f_{k+1/2,m}^{(\alpha+1/2)} - f_{k-1/2,m}^{(\alpha+1/2)}\right] + \sigma_{eff,m} f_{k,m}^{(\alpha+1/2)} - \frac{1}{2}\sum_{m=1}^{N} \mathrm{w}_m \sigma_{s,eff,m} f_{k,m}^{(\alpha+1/2)}$$

$$= \frac{1}{2}\sum_{m=1}^{N} \mathrm{w}_m \sigma_{s,eff,m} \Upsilon_{eff,k,m}^{(\alpha+1/2)} - \frac{1}{2}\sum_{m=1}^{N} \mathrm{w}_m \sigma_{s,eff,m} \Upsilon_{eff,k,m}^{(\alpha)} . \qquad (115)$$

As in Section 5.1, we approximate f with a two-term Legendre polynomial expansion

$$f_{k,m}^{(\alpha+1/2)} \cong \frac{1}{2} F_k^{(\alpha+1/2)} + \frac{3}{2}\mu_m J_k^{(\alpha+1/2)} , \qquad (116)$$

where

$$F_k^{(\alpha+1/2)} = \sum_{m=1}^{N} \mathrm{w}_m f_{k,m}^{(\alpha+1/2)} ,$$

$$J_k^{(\alpha+1/2)} = \sum_{m=1}^{N} \mathrm{w}_m \mu_m f_{k,m}^{(\alpha+1/2)} .$$

We thus rewrite (115)

$$\frac{\mu_m}{\Delta x}\left[\frac{1}{2}F_{k+1/2}^{(\alpha+1/2)} + \frac{3}{2}\mu_m J_{k+1/2}^{(\alpha+1/2)}\right] - \frac{\mu_m}{\Delta x}\left[\frac{1}{2}F_{k-1/2}^{(\alpha+1/2)} + \frac{3}{2}\mu_m J_{k-1/2}^{(\alpha+1/2)}\right]$$

$$+\sigma_{eff,m}\left[\frac{1}{2}F_k^{(\alpha+1/2)} + \frac{3}{2}\mu_m J_k^{(\alpha+1/2)}\right] - \frac{1}{2}\sum_{m=1}^{N} \mathrm{w}_m \sigma_{s,eff,m}\left[\frac{1}{2}F_k^{(\alpha+1/2)} + \frac{3}{2}\mu_m J_k^{(\alpha+1/2)}\right]$$

$$= \frac{1}{2}\sum_{m=1}^{N} \mathrm{w}_m \sigma_{s,eff,m} \Upsilon_{eff,k,m}^{(\alpha+1/2)} - \frac{1}{2}\sum_{m=1}^{N} \mathrm{w}_m \sigma_{s,eff,m} \Upsilon_{eff,k,m}^{(\alpha)} . \qquad (118)$$

However, since μ is an odd-function, we can immediately simplify (118),

$$\frac{\mu_m}{\Delta x}\left[\frac{1}{2}F_{k+1/2}^{(\alpha+1/2)} + \frac{3}{2}\mu_m J_{k+1/2}^{(\alpha+1/2)}\right] - \frac{\mu_m}{\Delta x}\left[\frac{1}{2}F_{k-1/2}^{(\alpha+1/2)} + \frac{3}{2}\mu_m J_{k-1/2}^{(\alpha+1/2)}\right]$$

$$+\sigma_{eff,m}\left[\frac{1}{2}F_k^{(\alpha+1/2)} + \frac{3}{2}\mu_m J_k^{(\alpha+1/2)}\right] - \frac{1}{2}\sigma_{s,eff,0} F_k^{(\alpha+1/2)}$$

$$= \frac{1}{2}\sum_{m=1}^{N} \mathrm{w}_m \sigma_{s,eff,m} \Upsilon_{eff,k,m}^{(\alpha+1/2)} - \frac{1}{2}\sum_{m=1}^{N} \mathrm{w}_m \sigma_{s,eff,m} \Upsilon_{eff,k,m}^{(\alpha)} , \qquad (119)$$

where for the discretized calculations, the 0th angular moments of the cross-sections are defined as, for example,

$$\sigma_{s,eff,0} = \frac{\sum_{m=1}^{N} \mathrm{w}_m \sigma_{s,eff,m}}{\sum_{m=1}^{N} \mathrm{w}_m}, \tag{120}$$

and

$$F_k^{(\alpha+1/2)} = \sum_{m=1}^{N} \mathrm{w}_m f_{k,m}^{(\alpha+1/2)}, \tag{121a}$$

$$J_k^{(\alpha+1/2)} = \sum_{m=1}^{N} \mathrm{w}_m \mu_m f_{k,m}^{(\alpha+1/2)}. \tag{121b}$$

Step 2: We proceed by taking the 0th angular moment of (119) and (114)

$$\frac{1}{\Delta x}\left[J_{k+1/2}^{(\alpha+1/2)} - J_{k-1/2}^{(\alpha+1/2)}\right] + \sigma_{a,eff,0} F_k^{(\alpha+1/2)}$$

$$= \sum_{m=1}^{N} \mathrm{w}_m \sigma_{s,eff,m} \Upsilon_{eff,k,m}^{(\alpha+1/2)} - \sum_{m=1}^{N} \mathrm{w}_m \sigma_{s,eff,m} \Upsilon_{eff,k,m}^{(\alpha)}, \tag{122}$$

and

$$F_k^{(\alpha+1/2)} = \frac{1}{2}\left[F_{k-1/2}^{(\alpha+1/2)} + F_{k+1/2}^{(\alpha+1/2)}\right]. \tag{123}$$

Step 3: We evaluate the 1st angular moment of (119) and (114)

$$\frac{1}{3\Delta x}\left[F_{k+1/2}^{(\alpha+1/2)} - F_{k-1/2}^{(\alpha+1/2)}\right] + \sigma_{eff,2} J_k^{(\alpha+1/2)} = 0, \tag{124}$$

and

$$J_k^{(\alpha+1/2)} = \frac{1}{2}\left[J_{k-1/2}^{(\alpha+1/2)} + J_{k+1/2}^{(\alpha+1/2)}\right]. \tag{125}$$

Here, we define

$$\sigma_{eff,2} = \frac{3\sum_{m=1}^{N} \mathrm{w}_m \mu_m^2 \sigma_{eff,m}}{\sum_{m=1}^{N} \mathrm{w}_m}, \tag{126}$$

Step 4: Collapse the system to a single equation. For convenience, we first define

$$\Theta_k^{(\alpha+1/2)} = \sum_{m=1}^{N} \mathrm{w}_m \sigma_{s,eff,m} \Upsilon_{eff,k,m}^{(\alpha+1/2)} - \sum_{m=1}^{N} \mathrm{w}_m \sigma_{s,eff,m} \Upsilon_{eff,k,m}^{(\alpha)} . \tag{127}$$

Add (119) for zones k and $k+1$

$$\left[J_{k+3/2}^{(\alpha+1/2)} - J_{k-1/2}^{(\alpha+1/2)}\right] + \Delta x \sigma_{a,eff,0} F_k^{(\alpha+1/2)} + \Delta x \sigma_{a,eff,0} F_{k+1}^{(\alpha+1/2)}$$

$$= \Delta x \Theta_k^{(\alpha+1/2)} + \Delta x \Theta_{k+1}^{(\alpha+1/2)} , \tag{128}$$

then add and subtract $J_{k+1/2}^{(\alpha+1/2)}$ to the $[\cdot]$ term

$$\left[J_{k+3/2}^{(\alpha+1/2)} - J_{k+1/2}^{(\alpha+1/2)}\right] - \left[J_{k+1/2}^{(\alpha+1/2)} - J_{k-1/2}^{(\alpha+1/2)}\right] + \Delta x \sigma_{a,eff,0} F_k^{(\alpha+1/2)} + \Delta x \sigma_{a,eff,0} F_{k+1}^{(\alpha+1/2)}$$

$$= \Delta x \Theta_k^{(\alpha+1/2)} + \Delta x \Theta_{k+1}^{(\alpha+1/2)} . \tag{129}$$

Rearrange (124) for an equation similar to Fick's Law:

$$J_k^{(\alpha+1/2)} = -\frac{1}{3\Delta x \sigma_{eff,2}} \left[F_{k+1/2}^{(\alpha+1/2)} - F_{k-1/2}^{(\alpha+1/2)}\right] , \tag{130}$$

or, utilizing the diamond-difference relationships of (125),

$$\left[J_{k-1/2}^{(\alpha+1/2)} + J_{k+1/2}^{(\alpha+1/2)}\right] = -\frac{2}{3\Delta x \sigma_{eff,2}} \left[F_{k+1/2}^{(\alpha+1/2)} - F_{k-1/2}^{(\alpha+1/2)}\right] . \tag{131}$$

Finally, substituting (131) into (129) and also using (123) yields the discretized diffusion equation

$$-\frac{1}{3\Delta x \sigma_{eff,2}} \left[F_{k+3/2}^{(\alpha+1/2)} - F_{k+1/2}^{(\alpha+1/2)}\right] + \frac{1}{3\Delta x \sigma_{eff,2}} \left[F_{k+1/2}^{(\alpha+1/2)} - F_{k-1/2}^{(\alpha+1/2)}\right]$$

$$+\frac{1}{4}\Delta x \sigma_{a,eff,0} F_{k+3/2}^{(\alpha+1/2)} + \frac{1}{2}\Delta x \sigma_{a,eff,0} F_{k+1/2}^{(\alpha+1/2)} + \frac{1}{4}\Delta x \sigma_{a,eff,0} F_{k-1/2}^{(\alpha+1/2)}$$

$$= \frac{1}{2}\Delta x \Theta_k^{(\alpha+1/2)} + \frac{1}{2}\Delta x \Theta_{k+1}^{(\alpha+1/2)} . \tag{132}$$

We note that (132) is a three-point stencil for correction factors, F, at cell-edges $k-1/2$, $k+1/2$, and $k+3/2$. A variety of linear solvers could be employed to solve

this tridiagonal system. The resulting correction factors, $F_k^{(\alpha+1/2)}$, are then used to correct and update $\Upsilon_{eff,k,m}^{(\alpha+1)}$

$$\sum_{m=1}^{N} \mathrm{w}_m \sigma_{s,eff,m} \Upsilon_{eff,k,m}^{(\alpha+1)} = \sum_{m=1}^{N} \mathrm{w}_m \sigma_{s,eff,m} \Upsilon_{eff,k,m}^{(\alpha+1/2)} + \frac{1}{2} F_k^{(\alpha+1/2)} \sum_{m=1}^{N} \mathrm{w}_m \sigma_{s,eff,m} . \quad (133)$$

Table 5 contains results from the coarse-grid DSA scheme compared with the Fourier analysis. The errors, most noticeably in cases 2 and 5, could be consequences of any errors from the fine-grid calculations. These errors could then carry over and influence the coarse-grid results. As in Section 3.4.2 and Section 4.4.2, the discretized computational spectral radii are less than the corresponding analytic spectral radii. This is principally due to the approximation of the infinite slab medium.

Table 5: Performance of the coarse-grid DSA scheme

case #:	accelerated theoretical $\lvert\rho\rvert$:	accelerated computational $\lvert\rho\rvert$:	relative error [%]:
1	0.180038	0.17282	-4.00915
2	0.025340	0.01470	-41.98895
3	0.153975	0.14665	-4.75727
4	0.237271	0.22913	-3.43110
5	0.096444	0.05254	-45.52279
6	0.153975	0.14665	-4.75727
7	0.192683	0.18496	-4.00814
8	0.024467	0.02446	-0.02861
9	0.153975	0.14781	-4.00390

6 CONCLUSION

In this study, we have presented several key components to deterministically solve neutral particle transport equations in binary stochastic media. Here, the underlying objective is to formulate transport equations for ensemble-averaged quantities (angular and scalar fluxes) and higher statistical moments (variance). We first derive the Adams-Larsen-Pomraning coupled stochastic transport model from the standard Boltzmann transport equation with an emphasis on particle conservation across an interface. This model is formally exact until we apply a simple approximation to close the system. Although the model was developed for arbitrary statistics, we assume the mixing statistics are known and can be described through homogeneous Markov processes.

In Section 3, we then proposed three candidate iteration schemes to solve the one-dimensional Adams-Larsen-Pomraning coupled model for the ensemble-averaged scalar flux unknowns. Our Fourier analyses of the three iteration schemes suggest that only two of three methods are stable and convergent. As we applied a variety of physical data to the partially- and fully- implicit iteration schemes, we predicted the convergence behavior and effectiveness by calculating the spectral radius of each method. The theoretical results were verified with computational results from an implementation code. For all nine test cases, the spectral radii for both methods correspond to the eigenvalue of the Fourier flat mode ($\lambda = 0$). In some cases, most notably where the optically-thick material is purely- or highly- scattering, we found that both iteration schemes can converge slowly. For the partially-implicit case, we were unable to determine the spectral radius of the entire method since nested iteration loops were required: a loop over the scattering term, and another over the coupling terms. On the other hand, we can solve the fully-implicit scheme with Source Iteration and without a nested iteration loop structure. The spectral radius

of the entire scheme can be measured directly, and we therefore infer that the fully-implicit method is the preferred iteration scheme. However, since Source Iteration is prone to slow convergence behavior in the presence of large amounts of scattering, an acceleration scheme is necessary to solve the highly scattering test cases.

Adams and Morel [BAda 93] originally developed a two-grid acceleration scheme for the multigroup S_N neutron transport equations with upscattering. In Section 4, we draw the analogy of our two material system to that of a two energy-group transport problem, deriving an acceleration scheme based on the Adams and Morel two-grid technique. The premise of this two-grid acceleration is to devise a low-order (coarse-grid) approximation to the original (fine-grid) coupled transport system. A spectral shape function, in the form of an eigenvector corresponding to the largest eigenvalue of the fine-grid iteration scheme, weights the "effective" cross-sections of the coarse-grid transport equation. The coarse-grid solution is subsequently used to correct the updated value of the ensemble-averaged quantities. However, unlike the two-grid system of Adams and Morel, our fine- and coarse- grid operators both involve transport equations. Our theoretical and computational results indicate that this two-grid acceleration scheme provides an effective and efficient means for accelerating the convergence rate of the fully-implicit method for, at least, the nine test cases. The analyses show that the accelerated spectral radii are not guaranteed to occur at the same Fourier mode as the unaccelerated spectral radii. In fact, the accelerated spectral radii now correspond to intermediate and higher frequency error modes since the two-grid acceleration successfully attenuates the unaccelerated low-frequency eigenvalues. While we see significant acceleration in many test cases, the degree of improvement is dependent on the material properties.

The coarse-grid solution requires a transport calculation, and is thus also vulnerable to slow convergence if scattering is present in one or both materials. Diffusion synthetic acceleration (DSA), applied appropriately, is a robust, unconditionally sta-

ble method to accelerate such transport calculations with highly scattering regions. For each iteration, a transport sweep is followed by a low-order diffusion calculation. The diffusion solutions are correction factors to update the coarse-grid transport sweep solutions. In Section 5, we illustrate the development of the coarse-grid diffusion synthetic acceleration system of equations. Using Larsen's 4-step method, we then obtain the discretized form of the 3-point diffusion equation. The analytic and discretized Fourier analyses show that the coarse-grid DSA spectral radii are, for most cases, much less than 1.0. Implementing DSA will be vital for further analysis of the two-grid system when the effective scattering ratio is close to unity.

We have made several restrictions in these studies. Although our model describes *neutral* particle transport in stochastic media, future studies could extrapolate the model for other types of radiation transport, including charged particles. Furthermore, we have only considered a background of two materials, but realistically, a medium could be composed of an arbitrary number of materials where each material has a corresponding transport equation. The model itself is not limited to two: for N materials, the coupled system would contain N equations with N coupling terms in each.

Our derivation of the coupled stochastic model assumes the special case of homogeneous Markov mixing statistics. Other research has incorporated various non-Markovian statistical models. *Renewal theory*, for one, has been used to describe stochastic transport in a binary mixture. Moreover, the mean chord lengths may not be exponentially distributed as we have assumed.

Several aspects of the two-grid acceleration scheme still warrant further investigation. First, the low-order transport operator defines an "effectively-mixed" transport equation, and perhaps this operator could be an accurate approximation to the coupled stochastic transport problem. For our two-grid scheme, we employ *transport* operators on both grids. If one, or both, grids could instead use *diffusion* operators,

the overall two-grid computational cost will decrease. The transport operators must perform transport sweeps, an iteration on the scattering term, and a diffusion calculation (DSA). Conversely, the diffusion operators simply require a linear algebra solver.

Further exploration into neutron transport in multi-dimensional stochastic geometries is also necessary for realistic applications. This includes the analysis of iteration schemes, as well as the generation of multi-dimensional transport benchmark calculations. In two-dimensions, realizations of Markovian statistics involve polygonal meshes [Har 84]. In three-dimensions, polyhedral grid transport algorithms will be necessary. This is a non-trivial extension of our work and is left as future work.

BIBLIOGRAPHY

[BAda 93] Adams, B.T., Morel, J.E., (1993), A Two-Grid Acceleration Scheme for the Multigroup S_n Equations with Neutron Upscattering, Nucl. Sci. Eng., **115**, 253.

[MAda 89] Adams, M.L., et al., (1989), Benchmark Results for Particle Transport in a Binary Markov Statistical Medium, JQSRT, **42**, 253.

[Arr 97] Arridge, S.R., Hebden, J.C., (1997), Optical Imaging in Medicine: II. Modelling and Reconstruction, Phys. Med. Biol., **42**, 841.

[Chi 00] Ching, B.S., Palmer, T.S., (2000), Analysis of Iterative Schemes for Binary Stochastic Mixture Transport Equations, Trans. Am. Nucl. Soc., **82**, 148.

[Gu 95] Gu, Y., et al., (1995), Radiative Transfer in Stochastic Media, The Astrophysical Journal, **450**, 318.

[Har 84] Harbaugh, J.W., Lin, C., (1984), Graphic Display of Two- and Three- Dimensional Markov Computer Models in Geology, Van Nostrand Reinhold, New York.

[Lar 82] Larsen, E.W., (1982), Unconditionally Stable Diffusion-Synthetic Acceleration Methods for the Slab Geometry Discrete Ordinates Equations. Part I: Theory, Nucl. Sci. Eng., **82**, 47.

[Lev 86] Levermore, C.D., et al., (1986), Linear Transport Theory in a Random Medium, J. Math. Phys., **27**, 2526.

[Mal 92] Malvagi, F., Pomraning, G.C., (1992), A Comparison of Models for Particle Transport Through Stochastic Mixtures, Nucl. Sci. Eng., **111**, 215.

[Mal 93] Malvagi, F., et al., (1993), Stochastic Radiative Transfer in a Partially Cloudy Atmosphere, J. Atmos. Sci., **50**, 2146.

[Pom 91] Pomraning, G.C., (1991), Transport Theory in Stochastic Mixtures, Trans. Am. Nucl. Soc., **64**, 286.

[Pom 86] Pomraning, G.C., (1986), Transport and Diffusion in a Statistical Medium, Transport Theory Statist. Phys., **15**, 773.

[Pom 89] Pomraning, G.C., (1989), Lecture Notes in Pure and Applied Mathematics (P. Nelson, editor), Vol. 115, 1-35.

[Pom 98] Pomraning, G.C., (1998), Transport in Discrete Stochastic Mixtures, Transport Theory Statist. Phys., **27(5-7)**, 405.

[Su 93] Su, B., Pomraning, G.C., (1993), Benchmark Results for Particle Transport in Binary Non-Markovian Mixtures, JQSRT, **50**, 211.

[Su 94] Su, B., Pomraning, G.C., (1994), A Stochastic Description of a Broken Cloud Field, J. Atmos. Sci., **51**, 1969.

[Tit 90] Titov, G.A., (1990), Statistical Description of Radiation Transfer in Clouds, J. Atmos. Sci., **47**, 24.

[VanK 81] Van Kampen, N.G., (1981), Stochastic Processes in Physics and Chemistry, North Holland, Amsterdam.

[Zuev 95] Zuev, V.E., Titov, G.A., (1995), Radiative Transfer in Cloud Fields with Random Geometry, J. Atmos. Sci., **51**, 176.